THE UNIVERSITY OF MICHIGAN

INDUSTRY PROGRAM OF THE COLLEGE OF ENGINEERING

AN INVESTIGATION OF THE BEHAVIOR OF THE ACOUSTIC EMISSION FROM METALS AND A PROPOSED MECHANISM FOR ITS GENERATION

Anand B. L. Agarwal

A dissertation submitted in partial fulfillment
of the requirements for the degree of
Doctor of Philosophy in the
University of Michigan
1968

March, 1968

IP-815

To My Wife, Neera

ACKNOWLEDGMENTS

The author wishes to express his sincere and profound gratitude to Professors Julian R. Frederick and David K. Felbeck, Co-Chairmen of the doctoral committee, for their continuous encouragement and innumerable stimulating discussions throughout this study. Their critical review of the manuscript and candid remarks have been extremely helpful.

Thanks are due Professors Leland J. Quackenbush and Wilbur C. Bigelow, members of the doctoral committee, for their advice, assistance and interest in this work.

The author will forever remain indebted to Professor Herbert H. Alvord, member of the doctoral committee, for his alert supervision and counsel throughout the author's Ph.D. program.

The author thankfully appreciates the cooperation of the following:

The staff of the Machine Tool Laboratory of the Department of Mechanical Engineering for machining the specimens.

The National Science Foundation and the Department of Mechanical Engineering for providing the generous financial support.

Mr. N. Gowri Sankar for several stimulating discussions.

Mrs. Annise L. Burnor for typing the rough draft and the staff of the Industry Program of the College of Engineering for the final typing and printing of this dissertation.

Finally, the author wishes to thank his wife, Neera, for her admirable patience throughout the duration of this investigation, which coincided with the very first year of her stay in the United States, and with the author.

TABLE OF CONTENTS

TABLE OF CONTENTS (CONT'D)

LIST OF TABLES

LIST OF FIGURES

LIST OF FIGURES (CONT'D)

LIST OF FIGURES (CONT'D)

LIST OF APPENDICES

NOMENCLATURE

ΣE	cumulative emission count
ΣE_{ℓ}	cumulative load emission count
ΣE_{u}	cumulative unload emission count
Δs	stress delay
τ_{cr}	critical shear stress
G	shear modulus
b	Burgers vector
ℓ	length of the dislocation line
τ_{b}	back stress of the pile-up
n	number of dislocations in the pile-up
D	average glide distance
ϵ	strain

ABSTRACT

The purpose of this investigation was to detect the acoustic emission from metals during loading and unloading in an attempt to pinpoint the source and understand the fundamental mechanisms responsible for its generation.

Specimens of 99.99 percent purity aluminum, 1020 steel, 2024 and Alcoa 195 aluminum were loaded in uniaxial tension. A piezoelectric crystal transducer, PZT-5 was used as a detector in conjunction with an amplifying system in order to record the amplitude and the number of generated acoustic pulses as a function of the induced stress. The effect of microstructural variations through controlled heat treatment of the specimens on the emission behavior has been studied.

Substantial emission during loading has been detected from 99.99 percent purity aluminum and from solution-treated 2024 and Alcoa 195 polycrystalline aluminum grades only upon the first application of load. Load emission from 1020 steel appears to be coincident with the yield point. No significant load emission could be detected from the specimens of the materials tested in the cold-worked condition. Precipitation hardening of 2024 aluminum causes load emission activity to decrease. Overaging, however, tends to cause it to return.

These results indicate that the load emission may be due to the activation of Frank-Read sources of a certain minimum size. For the detection system used, the minimum loop length of the source that

can be detected has been estimated to be of the order of 10^{-4} cm. The model offers a reasonable explanation for the phenomenon called the "Kaiser effect," and is consistent with the existing work hardening theories.

Cumulative unload emission count has been found to depend upon the maximum stress reached, the volume of the stressed material, and the hardness. It appears to be independent of the surface area and surface finish. Unload emission behavior seems to be identical in tension and compression loading modes and thus appears to be related to shear stresses. These results do not lead to a consistent model for the explanation of the unload emission data, hence more work needs to be done to determine the source and mechanism responsible for the unload emission.

CHAPTER I

INTRODUCTION

1.1 General

Modern technology, particularly the space program, the aircraft industry, and the growing trend towards higher operating speeds and elevated temperatures have been putting a tremendous stress and strain on the material scientists and engineers. The performance of a device is often limited by the mechanical properties of the materials of which it is made. An unceasing search must therefore continue in order to better understand the mechanical behavior of materials.

In 1934 Orowan,[1] Taylor,[2] and Polanyi[3] independently suggested the existence of dislocations in metals in order to explain a large discrepancy between the theoretical and real strength of metals. For a long time there was a widespread disbelief about this view, but in recent years experiments have been performed that prove the existence and importance of dislocations.

The presence of billions of dislocations in a material, and the multiplicity of the processes which control their motion, render it almost impossible to keep track of each individual dislocation as it moves through a material during deformation. For this reason it is difficult to explain many aspects of material deformation behavior quantitatively. The power of the theory, however, lies in its ability to offer acceptable qualitative explanations for a very large number of real material deformation phenomena. Quantitative estimates have also been made by using an average and statistical approach, results of which agree with the observed values within an order of magnitude.

A considerable amount of work has been done in recent years in order to visually observe dislocations, measure their velocity, and study their motion during loading and unloading. The advent of the high voltage electron microscope, etch pit and decorating techniques, etc., have helped significantly in the understanding of the dislocation mechanisms. However, all of these techniques are applicable to the study of dislocations in a quasi-static state only. Developement of a technique to detect and measure dislocation motion during the actual deformation could be very helpful in bridging the gap between real behavior and the theoretical predictions. Interest in the study of the so-called phenomenon of acoustic emission has been stimulated by this idea. The generation of acoustic pulses when materials are deformed has become a well known phenomenon in recent years. The energy associated with these emissions is several orders of magnitude below the audible level, and this low level suggests that a micromechanism such as the dislocation motion may be a possible cause of the emissions.

During the last two decades, a substantial amount of research effort has been devoted to attempts to understand the source of these emissions. It is believed that when metals fail because of fatigue, yielding, or fracture, the failure is usually preceded by, or is dependent upon, the ease of movement of structural imperfections (dislocations) in the metal lattice. When these move suddenly, they make a noise which can be detected by a sensitive microphone attached to the metal. Hence investigations of acoustic emissions from metals as they are being stressed or unstressed seem to offer considerable eventual promise as a means of predicting their mechanical behavior.

1.2 Literature Review

Historically, the first indication that metals, upon being stressed, emit sound was made by the early tinsmiths. The sound emitted by the tin was called "tin cry" and could be heard by the unaided ear. Czochralski[36] suggested that the sound pulses were related to the twinning occurring in the tin.

Most pioneering work in the area of acoustic emission was reported in 1950 by Kaiser.[4] He observed stress-induced sound pulses from zinc, steel, aluminum, copper, lead and even wood. The amplitude of these emissions was so small that an electronic system to provide a large amplification had to be used in order to detect them. Kaiser concluded that the frequency and amplitude of emitted pulses were related to the stress level and the past history of the material. He found, for the first time, that on restressing a previously stressed material the emission did not begin until the previous stress was reached. This phenomenon later became known as the "Kaiser Effect," and has also been observed by other workers.[5,6]

Tatro and Liptai[5] worked with single and polycrystals of aluminum and suggested that the emission is a surface rather than a volume related phenomenon. They postulated that the surface oxide layer or the surface itself acts as a barrier to the motion of dislocations, thus resulting in a pileup. Detectable emission bursts are produced when the applied stress becomes large enough to cause the pileups to break-through, thereby releasing localized strain energy to provide new surface, heat and an elastic wave. They found that an oxide coated surface gives rise to a higher emission activity which

they thought is caused by a larger number of dislocations in the pileup before the surface barrier breaks down allowing the dislocations to egress.

Schofield[6] carried out some extensive investigations and suggested that the acoustic emission is a function of the basic deformation process. He observed that: (1) The emission activity increases with a decrease in the surface egress of dislocations, (2) annealed gold single crystals emit profusely and (3) aluminum single crystals rarely emit high energy pulses which are known as bursts. Based on these observations, he drew the following conclusions:

(1) The surface oxide layer itself is not an emission source, but the emission characteristics are significantly modified as a result of the influence of the oxide on the deformation behavior of the specimens. He also contradicted Tatro and Liptai's view that emissions are due to an interchange of energy when a slip step is formed on the surface of the specimen.

(2) Emissions are due to the repinning of dislocations rather than their unpinning. He argued that the high emission activity in an oxide coated specimen is associated with the high resistance of the surface to the dislocation mobility.

(3) The rarity of bursts from high purity aluminum and profuse emission from gold single crystals led him to believe that the development of stacking faults during the deformation process is the cause of high energy bursts. Since gold has low stacking fault energy, it produces more stacking faults and consequently more burst emissions.

Of all the work on acoustic emission, reported in the literature prior to 1965 there is only a brief mention by Schofield[6] of the existence of the emission that is observed when the applied stress is removed. The phenomenon of unload emission has been studied and reported for the first time, in detail, by Kerawalla[7] and Mitchell[8] in 1965. Since the present investigations are a continuation of the above studies, a rather detailed summary of their work is presented in the following paragraphs.

Acoustic emission that is obtained during loading and unloading a steel specimen in uniaxial tension consists of bursts of noise of various amplitudes. These bursts are reflected back and forth within the specimen and decay exponentially (see Figure 1.1). This gives each burst a characteristic frequency which corresponds to the resonant frequency of the test specimen.

In general, the cumulative total emission that occurs in steel during the application and removal of an axial tensile load varies in the manner shown in Figure 1.2. From A to B there is very little emission of noise. The increase in emission at B coincides with yielding of the specimen. As the stress continues to increase beyond the yield stress very little noise is observed even though the point C may lie beyond the stress which produces necking. When the load is gradually removed, no emission occurs until a stress corresponding to D is reached. Emission then occurs and continues until the stress becomes zero.

The number of bursts obtained on unloading the specimen is usually an order of magnitude greater than that which is obtained on loading. Furthermore, it is reproducible to within four percent on specimens with the same prior history.

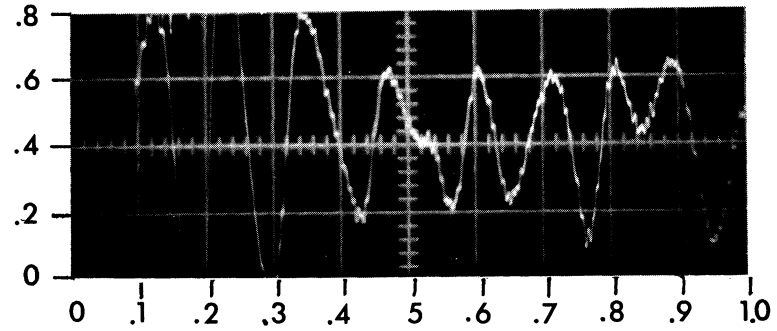

Figure 1.1 A Typical Acoustic Burst.[8]

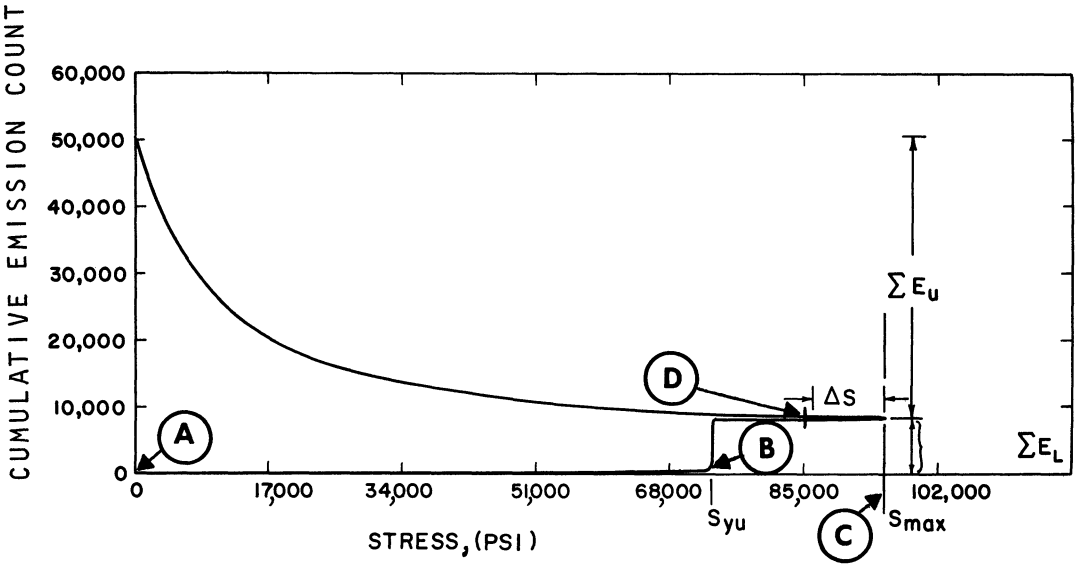

Figure 1.2 Dependence of the Cumulative Acoustic Emission in Steel on an Axial Tensile Stress.[8]

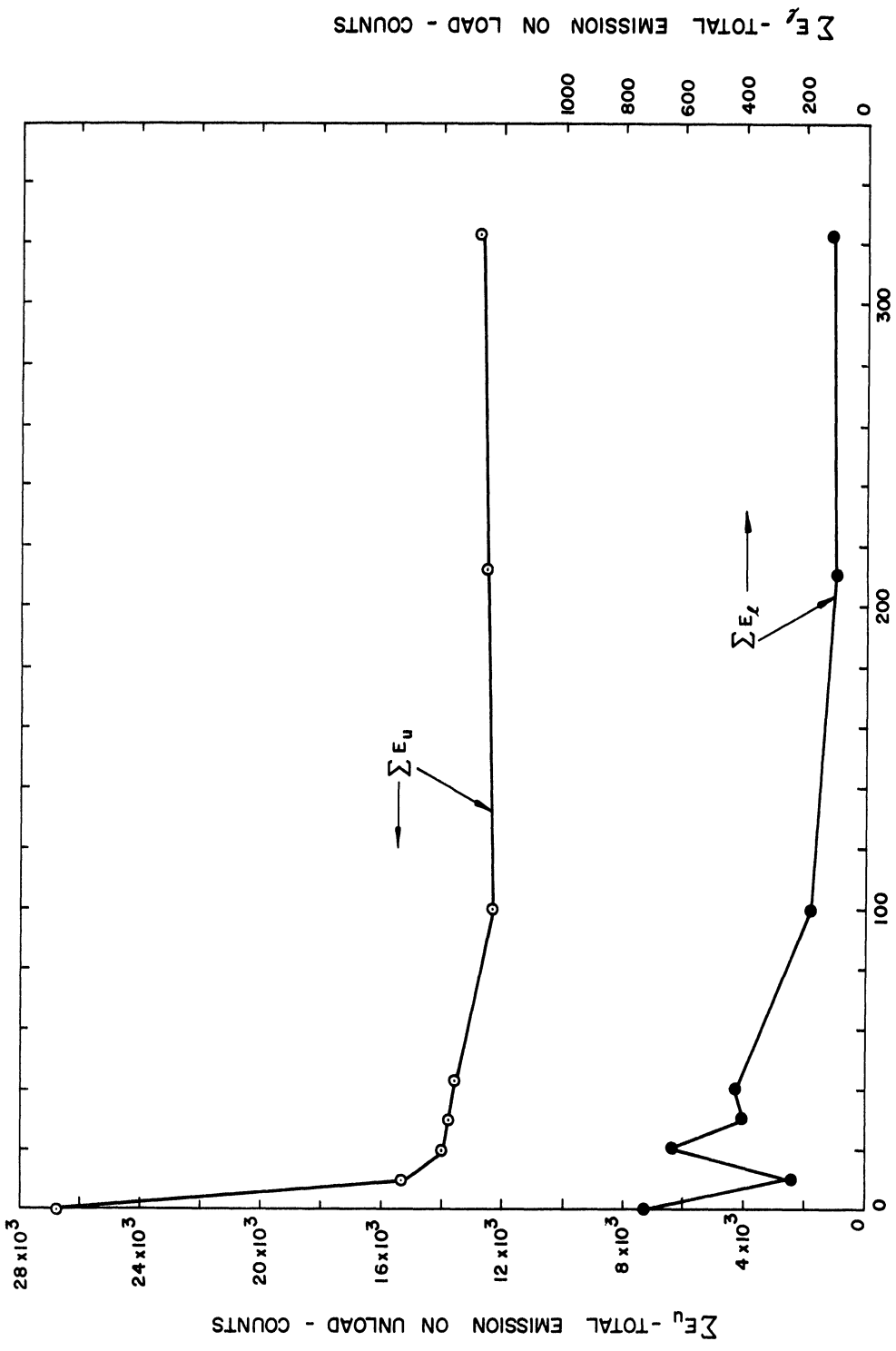

Figure 1.3 Effect of Strain Aging at Room Temperature on ΣE_u and ΣE_ℓ in 1045 Hot Rolled Steel.(7)

Strain aging effects have been observed to alter the acoustic emission from steel. The unload emission given off by a specimen is less when it is reloaded after a lapse of hours or days during which time it is left in the grips without any load. Specimens of 1020, 1045 and 4340 steel all show this effect. Figure 1.3 is a typical graph. It is believed that the diffusion of interstitial solute atoms causes an increased locking effect which results in a decreased unload emission count.

The cumulative unload emission depends on the peak stress reached in a given test as shown in Figure 1.4. In the experiments that have been performed on 1020 and 1040 steels by Kerawalla, the peak of the curve occurs at a stress which corresponds approximately to point B in Figure 1.2 and also to both the yield point in static tensile tests and the endurance limit in fatigue tests.

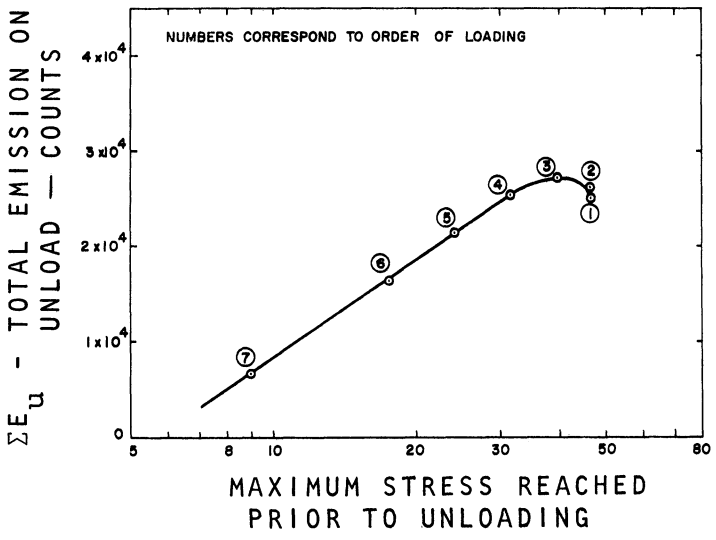

Figure 1.4 Dependence of the Unload Emission on the Maximum Stress Reached Prior to Unloading the Specimen.

Kerawalla[7] concluded that:

(1) The large load emission in 1020 annealed steel is due to the phenomenon of yield drop and yield elongation. Materials which have a smooth transition from elastic to plastic region do not give rise to such load emissions.

(2) Surface slip is not the cause of this emission.

(3) Twinning is not a cause of acoustic bursts.

(4) The load emission is caused by the unpinning of dislocations from the locking effect of carbon and nitrogen atoms.

(5) Emission pulses on unloading are a result of the sudden movement of dislocation lines or tangles. These movements are accompanied by abrupt change in line energy as well as potential energy of dislocations as they return to the position of minimum potential energy.

Mitchell[8] suggested that the unload emissions are intimately connected with the recoverable elastic behavior of the material.

Sedgwick[9] worked with coated and uncoated crystals of lithium flouride and potassium chloride and concluded that an avalanche of dislocations emanating from a Frank-Read source creates an elasto-plastic wave of sufficient energy to be picked up by the detection system. Release of dislocation pileups has been considered by Sedgwick to be a secondary source of acoustic bursts.

Fisher and Lally[10] have suggested that emission bursts are associated with tiny bursts of plastic strain, which are essentially microscopic yield points, resulting in load drops.

CHAPTER II

EXPERIMENTAL PROCEDURE

The equipment in this investigation was essentially the same as used by Kerawalla and Mitchell. Several modifications and additions have been made in order to adapt the test setup to the present study. A brief description of the testing facility is given in the following paragraphs.

2.1 Loading System

A specially designed low noise loading and unloading machine has been used throughout this study. The operation of this machine can be understood by referring to the schematic sketch in Figure 2.1 and photographs of Figures 2.2, 2.3, and 2.4 as follows. The load is applied to the specimen by lowering tank No. 1 by means of a synchronous motor driven pulley system. The lowering of this tank causes the water in tank No. 3 to be drained out, hence reducing the buoyant force on the sand ballast tank No. 2. The specimen thus supports the part of the weight of the ballast tank which is not balanced by the buoyant force through a 20:1 leverage. The magnitude of the load supported by the specimen is determined by the position of tank No. 1. The rate of loading can be varied by valve No. 1 which controls the rate of flow of water in and out of tank No. 3. The specimen is held in forked tension grips (Figure 2.4) which are pulled through a set of four self-aligning ball and socket joints. The grips are made of molded nylon polymer. Nylon grips have been found to provide excellent acoustic isolation of the specimen from the rest of the loading fixture.

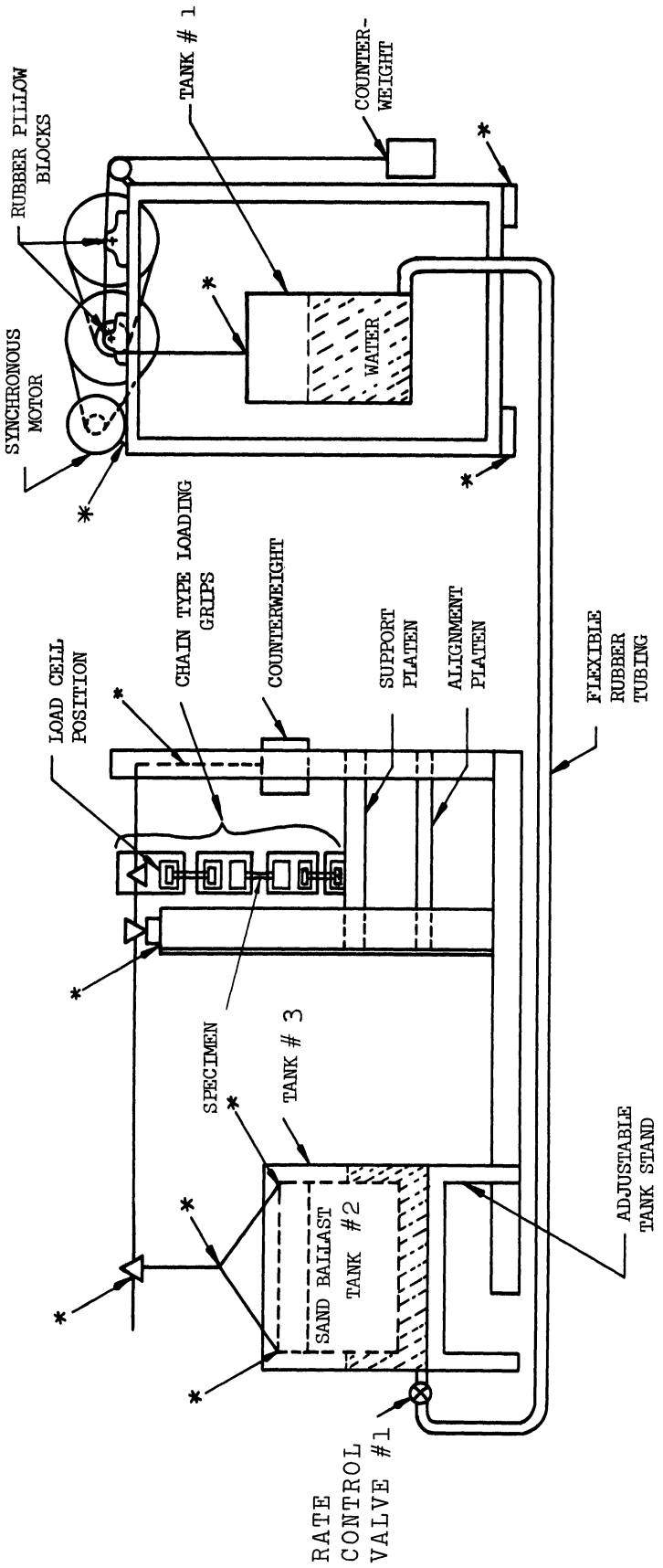

Figure 2.1 Schematic of the Acoustic Tensile Testing Machine.(8)

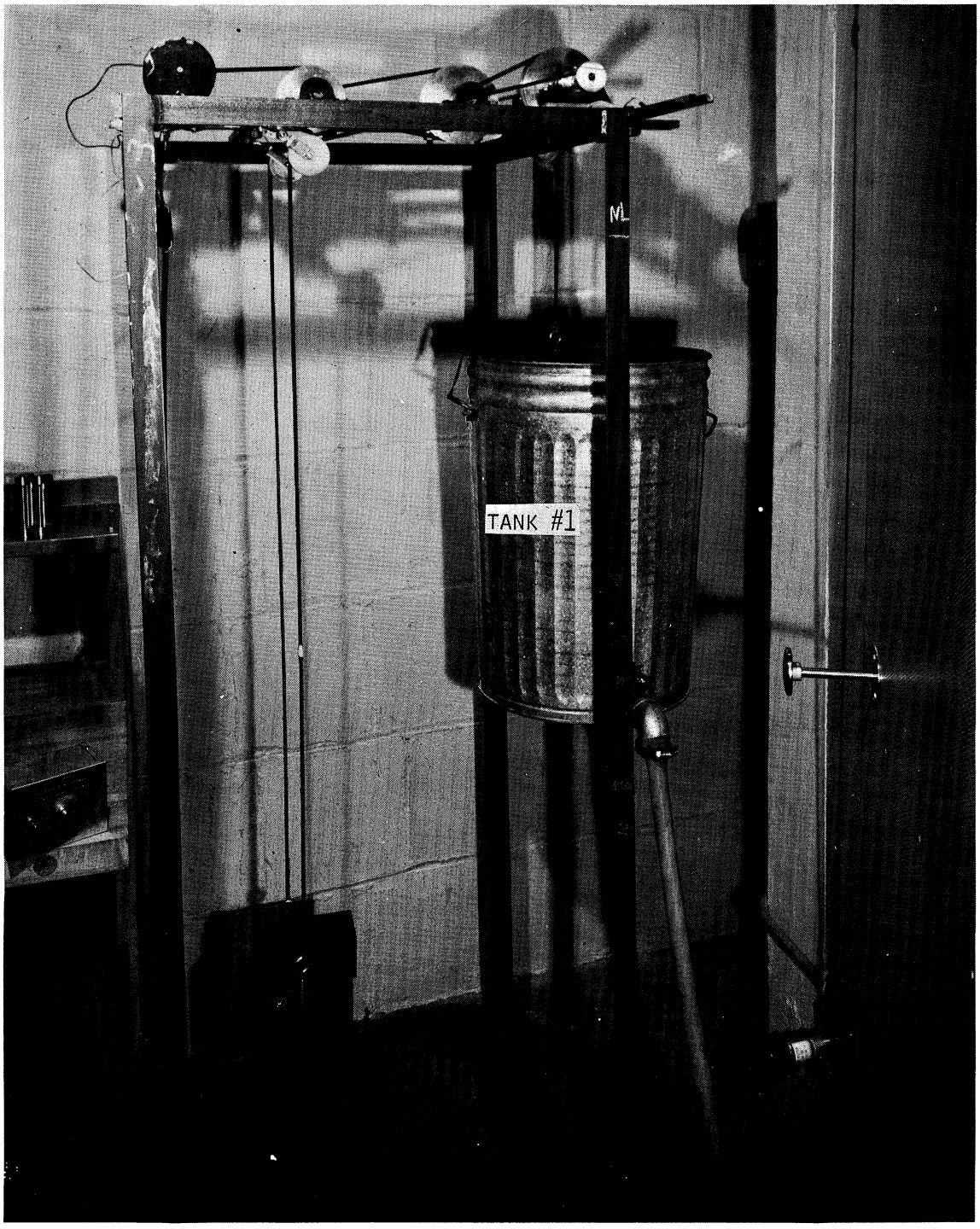

Figure 2.2 Tank 1 and Its Operating Mechanism.

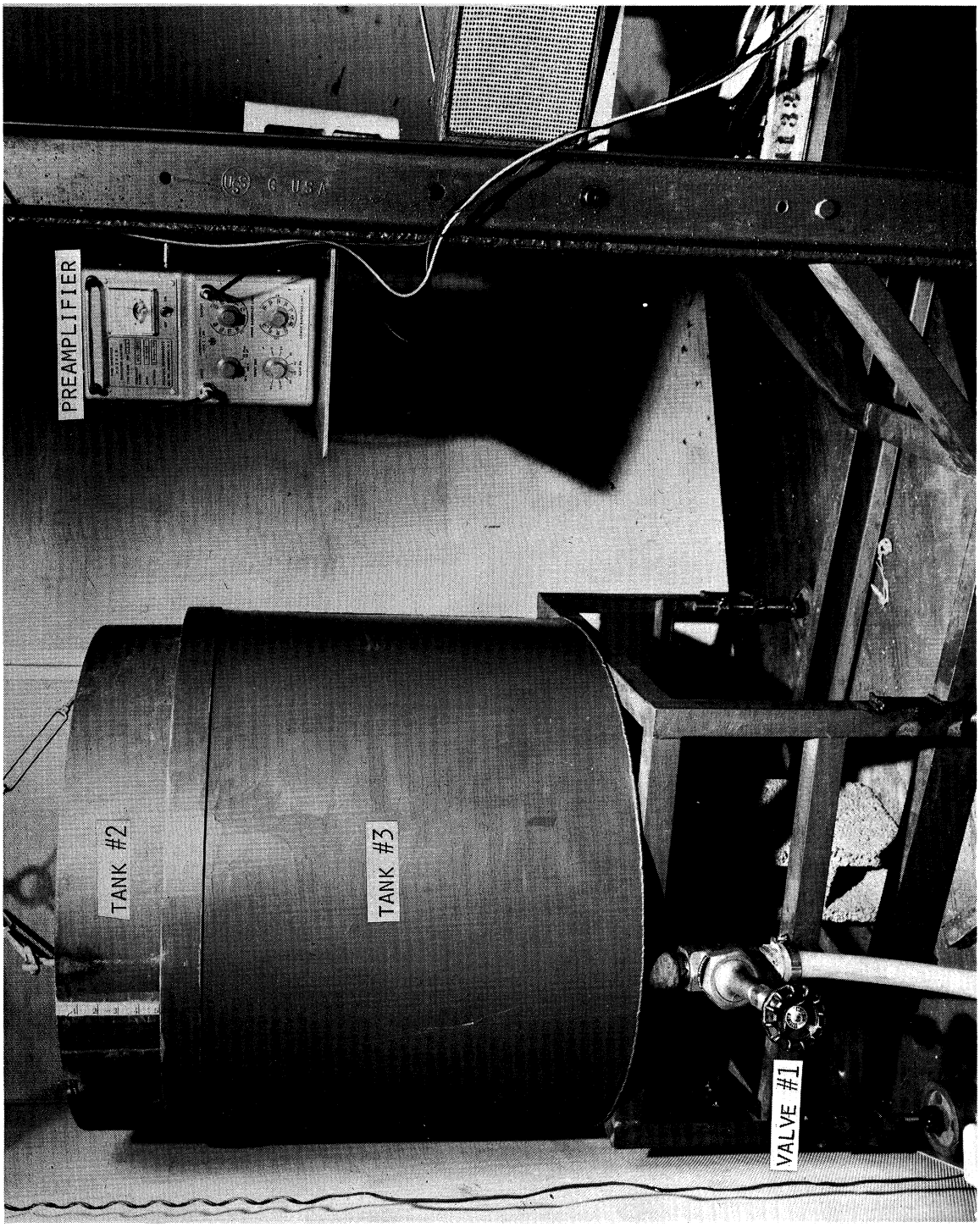

Figure 2.3 Float Tank and the Loading Rate Control Valve.

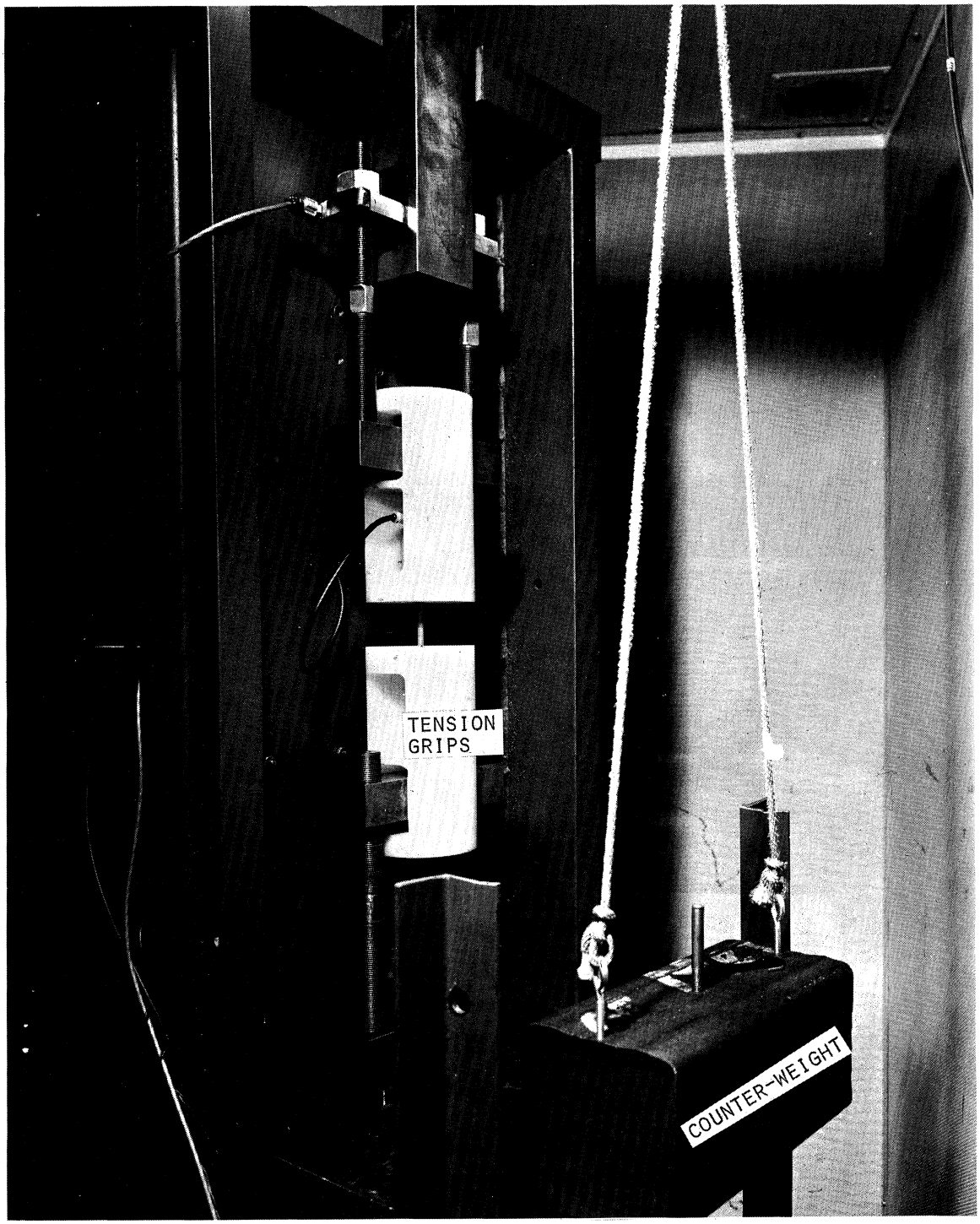

Figure 2.4 Tensile Loading.

The entire loading gear, with the exception of the tank No. 1 and its operating mechanism, is located in an Inudstrial Acoustic Company Model 402 A audiometric room which keeps the ambient noise level in the chamber at an acceptably low level.

The same loading system was adopted for applying compressive load on the specimen. The top nylon tension grip is removed and the compression specimen is supported on the movable cross-arm as shown in Figure 2.5. The specimen is pushed against an aluminum bracket rigidly attached to the frame thus applying desired compressive load that is measured by the same load cell as in the tension test. The ball joint on the crossarm helps align the specimen with respect to the line of action of the applied load.

A specimen carrying two sensitive semiconductor strain gages is used regularly to check for possible bending stresses induced due to misalignment of the load.

A semiconductor strain gage load cell is incorporated in the loading machine in order to measure the load applied to the specimen. This load cell has been calibrated against a certified load cell manufactured by Research Incorporated.

A soldering iron has been adapted so it can be clamped to the specimen in order to heat it within the grips while under load. The temperature was controlled by powering the iron through an autotransformer and adjusting the voltage. Care was taken not to heat specimens above 200°F in the nylon grips.

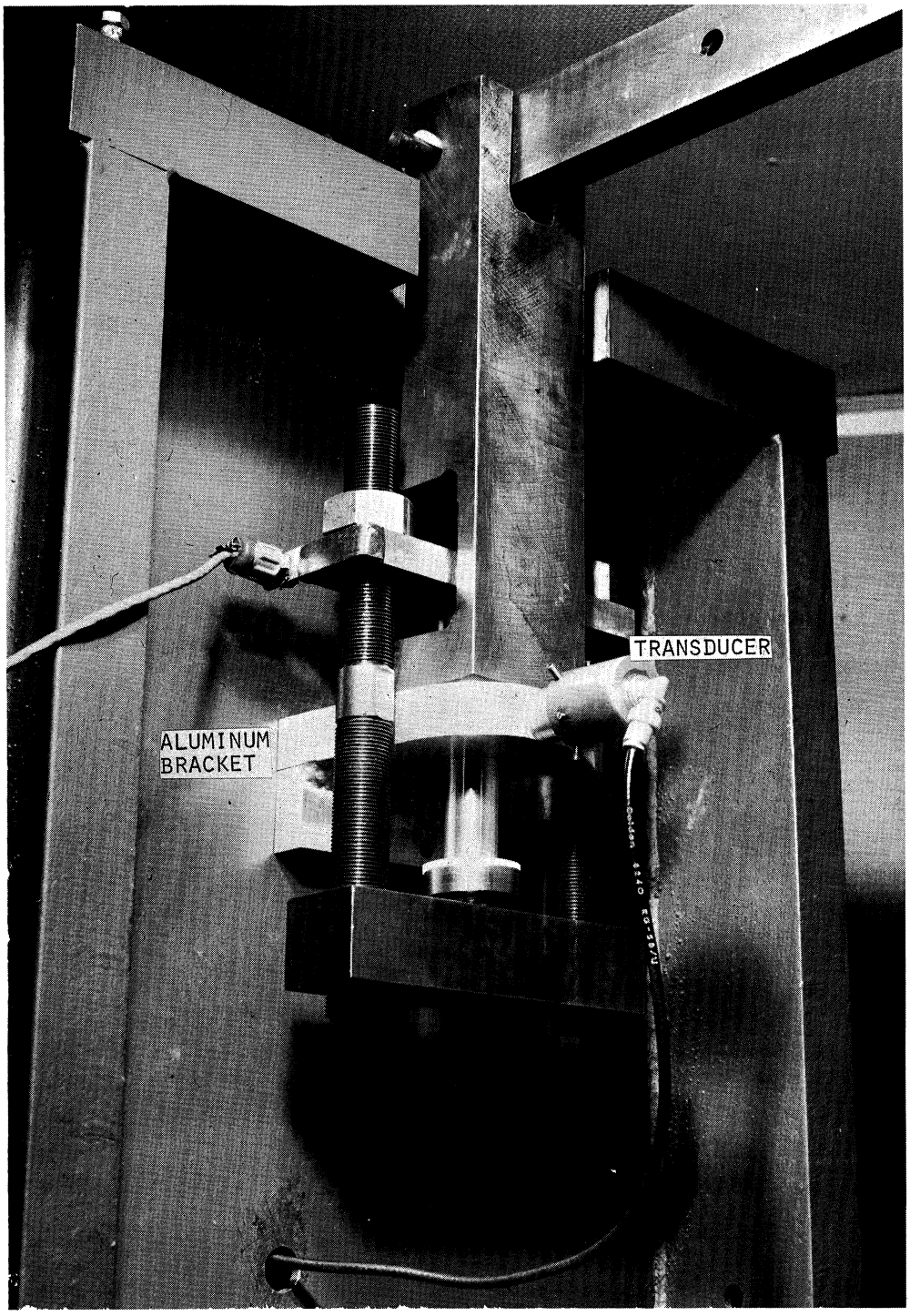

Figure 2.5. Compressive Loading.

2.2 Electronic Equipment

The block diagram of Figure 2.6 represents the complete instrumentation system used for the investigation. All of the electronic equipment with the exception of the crystal pick-up, the pick-up head, and the hushed preamplifier is located outside the audiometric chamber (see Figure 2.7).

The pick-up head maintains a uniform contact between the specimen and the crystal transducer, through an oil film and is clamped on to the specimen by three equi-spaced centering screws. In case of the compression loading the pick-up head is mounted on the aluminum bracket instead of the specimen itself. At the threshold levels used in the present investigation there is no significant difference in the sensitivity of the transducer when the pick-up head is held on to the specimen and when it is mounted on the aluminum bracket.

All tests were conducted using a lead zirconate titanate piezo-electric crystal (PZT-5) which was 0.25 inch diameter and 0.1 inch thick. The crystal pick-up is connected to a low noise "hushed" preamplifier by means of a very short cable. The output of the preamplifier is connected to an electrical filter which passes a band of frequencies from 2 kHz to 20 kHz. This narrow bandwidth has been used because it was found that most of the bursts picked up by the system have a frequency of about 10 kHz. This narrow bandwidth allows the use of a 80 db gain on the preamplifier.

The signal from the filter is connected in parallel to a vacuum tube voltmeter, a Tektronix oscilloscope, a loud-speaker, and to a digital-to-analog converter through an electronic counter. The counter records the total number of pulses which have a peak voltage greater

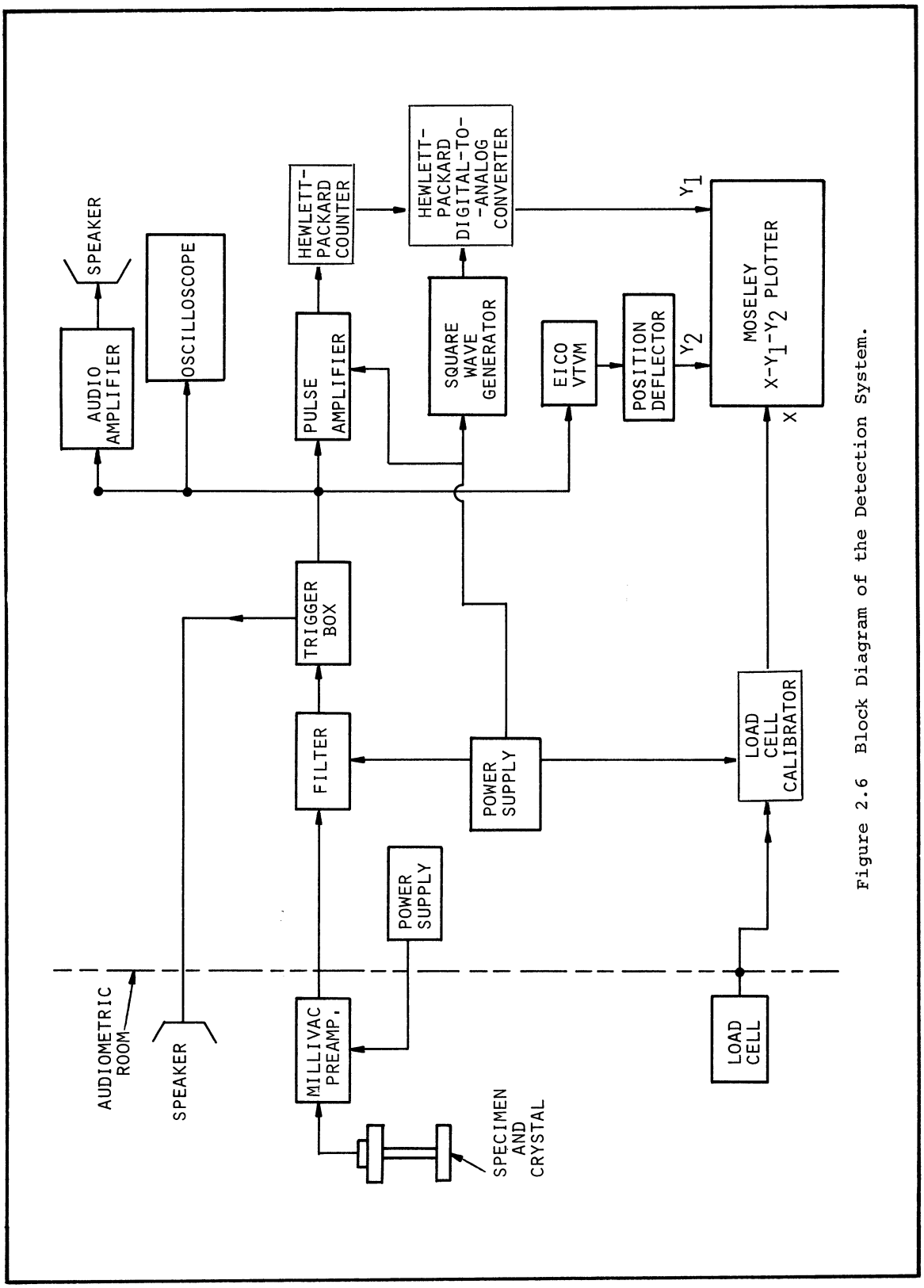

Figure 2.6 Block Diagram of the Detection System.

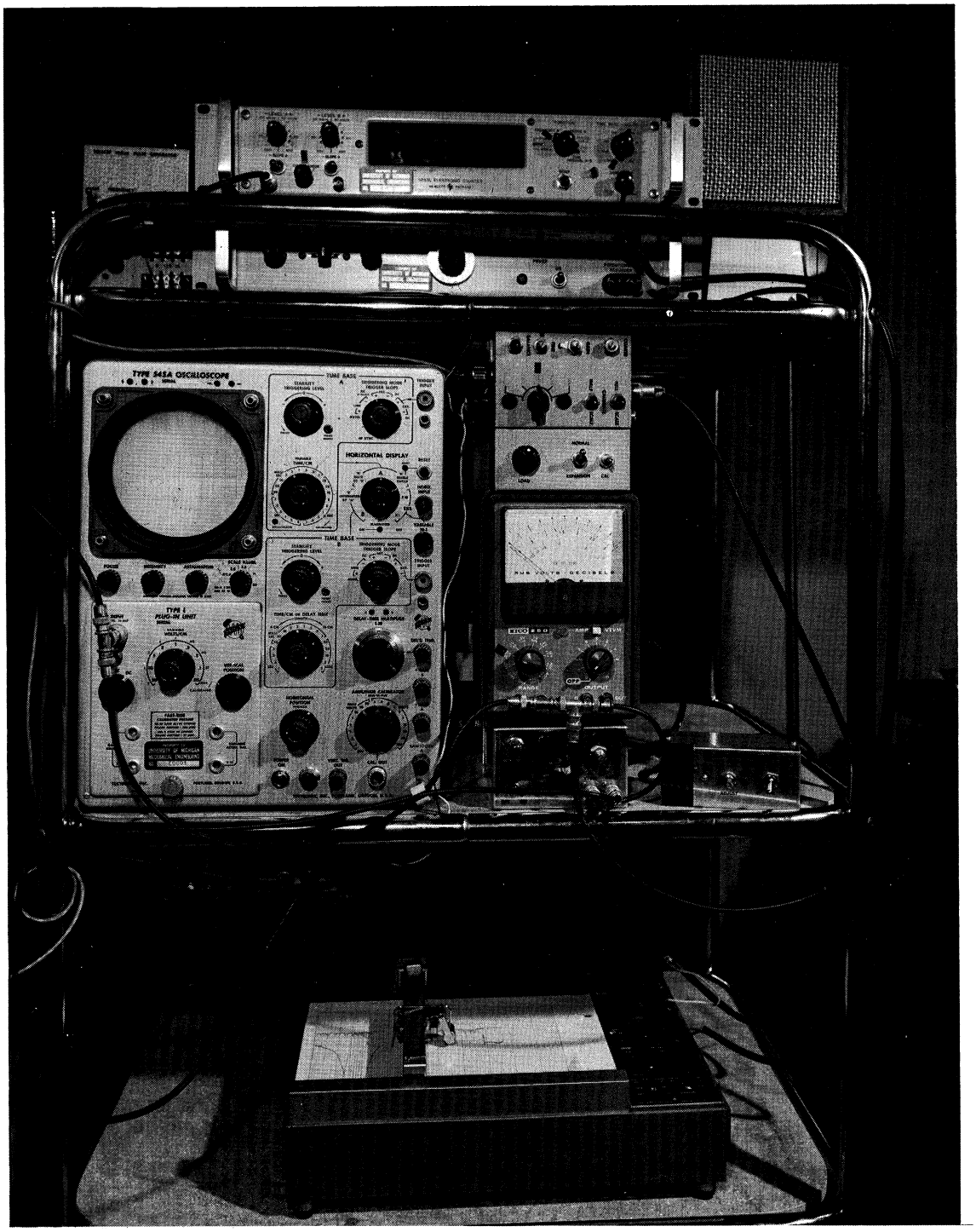

Figure 2.7 Electronic Instrumentation for the Detection of Acoustic Emissions.

than a predetermined threshold level. In order to set the trigger level of the counter with precision a standard voltage signal source is provided. This signal is fed to the counter and the trigger level is adjusted.

In order to check the overall calibration of the system including the acoustic coupling between the specimen and the crystal transducer, a random noise signal generator has been built. A standard noise signal is injected into the audiometric room and the output of the crystal is measured on the VTVM. Both the trigger circuit and the random noise generator are built into the same box which is labeled as the "Trigger Box" in the block diagram of Figure 2.6. The detection system can be conveniently switched from the normal operating position to the trigger-mode or set-mode without disturbing any other part of the setup.

An $X\text{-}Y_1\text{-}Y_2$ plotter is used to record the cumulative emission count and the intensity of acoustic pulses as a function of the load on the specimen. A position deflector switch is used to deflect the pen on the Y_2 channel of the recorder so that a separate, nonoverlapping record the amplitude of the emitted pulses could be obtained during loading and unloading.

A procedure for calibrating the $X\text{-}Y_1\text{-}Y_2$ plotter is included in Appendix I.

2.3 Test Procedure

The standardized test procedure given below has been followed throughout the test program.

The piezoelectric crystal transducer is seated into the pick-up head which is mounted on the flat-faced end of the specimen. The specimen

is then seated into the grips. The upper grip is then raised by turning the screws (Figure 2.4) until there is a small preload on the specimen. The audiometric room is then closed and the standard random noise signal is injected into it via a loud-speaker. The output of the transducer is fed through the preamplifier and filter and displayed on the VTVM. By rotating the pick-up head and varying the pressure between the specimen and the crystal, the same VTVM reading is obtained for various tests. This completes the acoustic coupling test. Next, the standard trigger-signal voltage is applied to the counter and the trigger level on the counter is adjusted until it just starts to count. This fixes the threshold level. The amplifier channels of the $X\text{-}Y_1\text{-}Y_2$ plotter are checked for calibration, using built-in calibration signals. Tank No. 1 is then lowered until maximum desired load on the specimen is reached. This is read on the X-channel of the recorder. The intensity and the cumulative count of the emitted pulses is recorded on the Y_2 and Y_1 channels, respectively. Tank No. 1 is raised in order to remove the load. The position deflector switch is set on the "ON" position, this deflects the Y_2 channel by about an inch on the chart.

2.4 Materials

In order to study the effect of the microstructure on the acoustic emission behavior that may be caused by variations in composition and heat treatment, several different materials have been used. Table II.1 gives the nominal compositions of these materials as reported by the manufacturers, except for the Alcoa 195 which was obtained from a commercial testing laboratory.

TABLE II.1

COMPOSITIONS OF MATERIALS USED

(a) Aluminum

Type	Cu	Fe	Si	V	Zn	Mn	Mg	Cr	Al
Hi Purity	0.003	0.004	0.001	0.001	0.001	----	----	----	bal.
2024	4.5	----	----	----	----	0.6	1.5	----	bal.
6061	0.25	----	0.6	----	----	----	1.0	0.25	bal.
Alcoa 195	5.0	0.2	0.5	----	0.20	0.50	0.10	0.10	bal.

(b) Steels

Type	C	Mn	P	S	Si	Cr	Ni	Fe
1020	.18-.23	.30-.60	.04	.05	---	---	---	bal.
1042	.40-.47	.60-.90	.04	.05	---	---	---	bal.
302	0.15	2.0	---	---	1.0	17.0-19.0	8.0-10.0	bal.

2.5 Specimen Preparation

All of the specimens were machined on a lathe in the as-received or in a heat-treated condition. No further surface finishing operation was performed. Figure 2.8 shows the shop drawings of the specimens used. Most of the specimens had a straight test section of uniform diameter but some had a gage section of reduced diameter in order to obtain a higher stress level for the same maximum applied load.

Care was taken to ensure that there was no extraneous noise from the rubbing of the float tank, or the rotation of the specimen within the grips. The procedure for doing this is described in Appendix II.

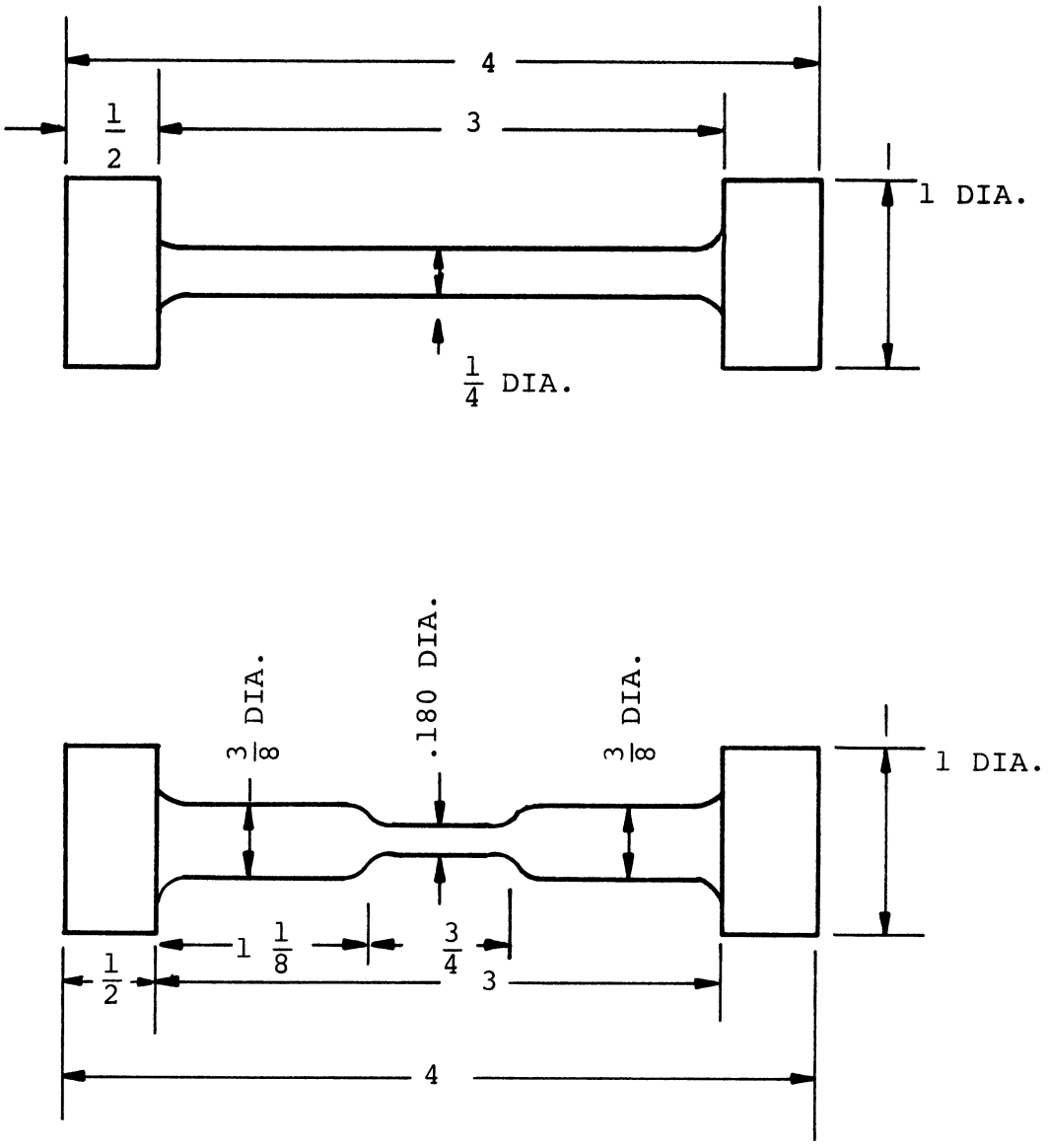

ALL FILLET RADII TO BE 0.1 INCH.
NO CENTER HOLE ON ONE END FACE
SMOOTH FINISH ALL OVER
DIMENSIONS IN INCHES

Figure 2.8 Test Specimens.

CHAPTER III

EXPERIMENTAL RESULTS

3.1 General Acoustic Emission Behavior

All of the acoustic emission data are presented as graphs of the cumulative emission count and the amplitude of emitted pulses as a function of the applied stress. Figure 3.1 shows a typical plot of the emission obtained from an as-received and machined 1042 steel specimen. During loading, acoustic pulses first appear at a very small stress and are random in character. When unloading begins, there is no emission until the load is reduced by several percent at which point bursts of large intensity begin to be emitted and continue until the applied stress becomes zero. The cumulative emission count upon unloading is always much larger than that during loading. Subsequent acoustic tests on the same specimen reveal practically zero emission during loading. The unload emission on a single specimen is reproducible within a few percent. This behavior is representative of all materials tested.

3.2 Unload Emission

3.2.1 Effect of the Surface Finish of the Specimen

Before any extensive testing was done, some preliminary experiments were performed to evaluate the possible effect of surface finish on the acoustic emission. These were done on 6061 aluminum and 1020 steel (see Table II.1 for composition) specimens which had been given various surface preparations. Results shown in Figure 3.2 indicate that the cumulative emission count on unload over a range

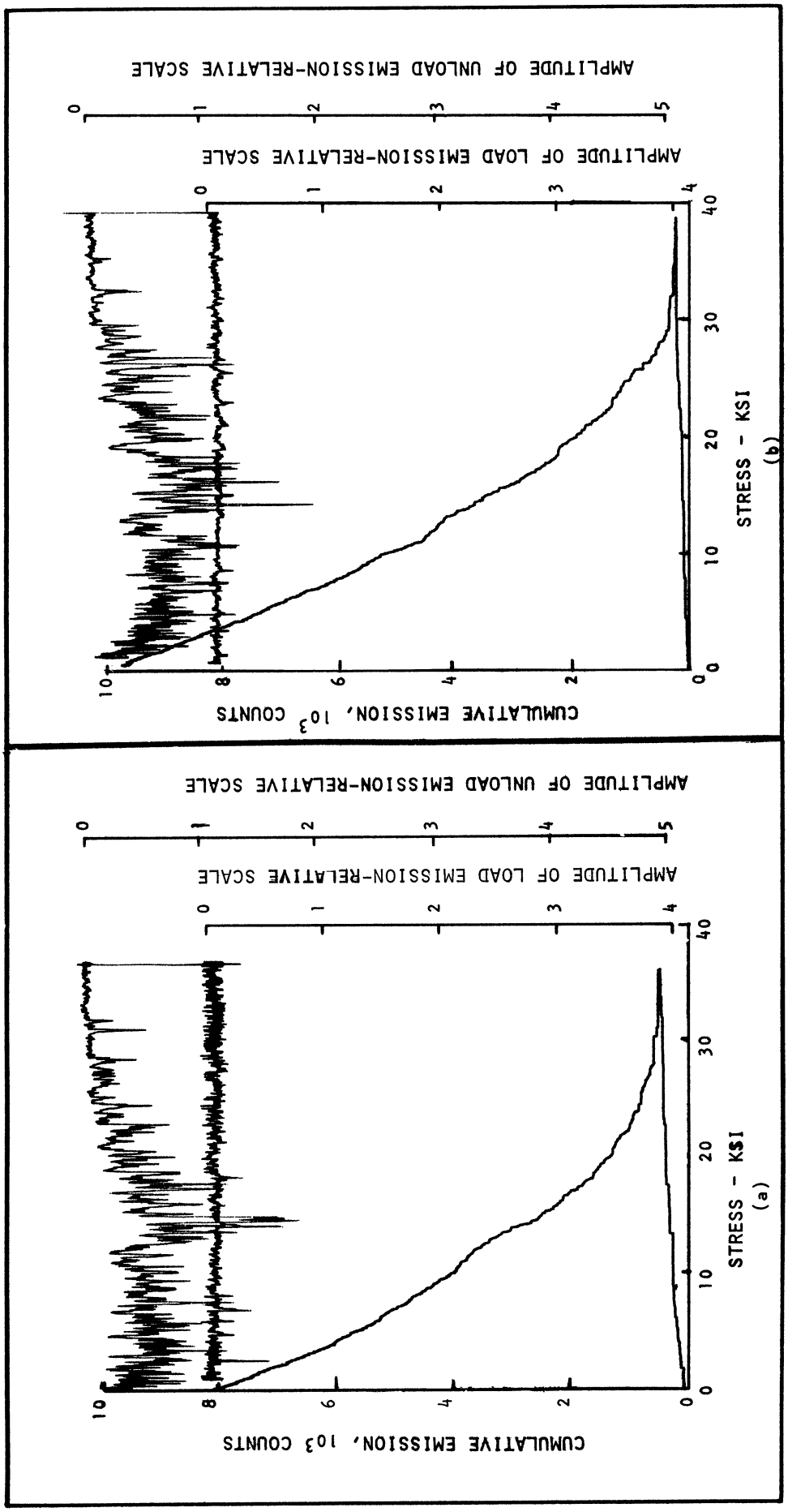

Figure 3.1 Emission from 1042 Steel (as received)
a) First Loading, b) Second Loading.

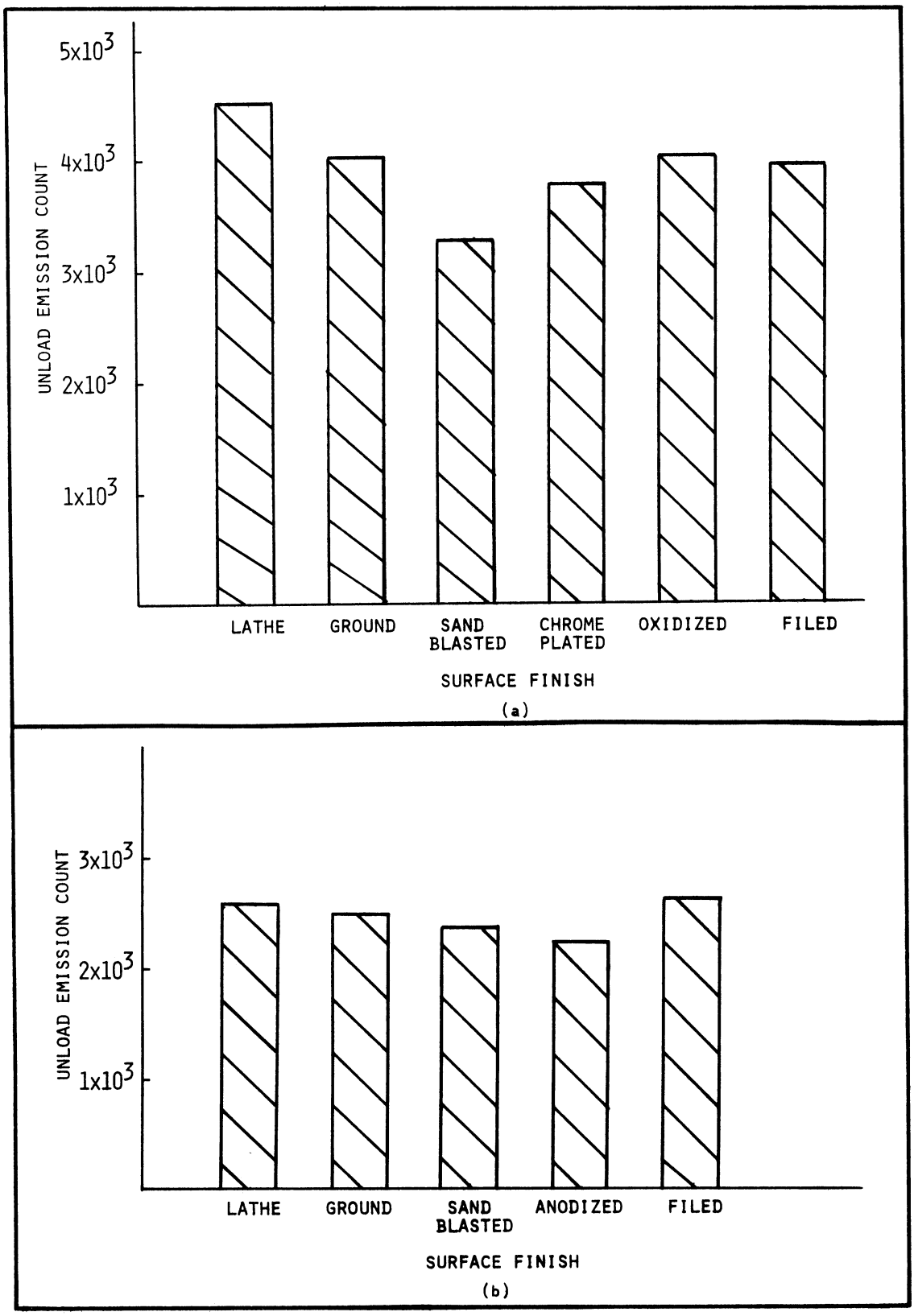

Figure 3.2 Effect of the Type of Surface Finish on the Unload Emission. a) 1020 Hot Rolled Steel, b) 6061-T6 Aluminum.

of surface finishes on 6061-T6 aluminum specimens is essentially the same. Likewise 1020 hot-rolled steel specimens with different surface finishes show an almost identical unload emission behavior. As a result of these tests it was concluded that the surface finish does not significantly affect the unload emission. All subsequent tests were, therefore, performed on specimens that were machined on a lathe.

3.2.2 Effect of the Surface Area and Volume of the Specimen

Since the unload emission count was little affected by the change in the surface finish of the specimens and since Tatro and Liptai (Reference 5) have suggested that emission is a surface and not a volume phenomenon it was felt desirable to conduct experiments to study the effect of the size of the test specimen.

Ten specimens of 6061-T6 aluminum were machined such that six of them had the same surface area but variable volume and four had the same volume but different surface area. Table III.1 shows the actual dimensions and the applied load on each specimen so that the same maximum stress of 23.5 ksi was induced in each of them. Cumulative unload emission count from these tests is plotted in Figure 3.3.

3.2.3 Effect of the Percent Cold-Work

In order to study the effect of the percent cold-work on the acoustic emission, nine cold-worked aluminum specimens were prepared from a single bar of Alcoa 195 alloy.

The specimens were all machined from a four inch square cross-section bar of annealed material which was reduced in cross-section by successive passes through a nine inch rolling mill in order to cold-work

TABLE III.1

APPLIED LOAD AND DIMENSIONS OF SPECIMENS USED TO STUDY THE EFFECT OF INDEPENDENT CHANGE IN THE SURFACE AREA AND VOLUME ON ACOUSTIC EMISSION

(a) Variable volume, constant area.

Specimen No.	Diameter in.	Length in.	Volume $(in.)^3$	Load lb.
1	0.200	4.50	V_o	750
2	0.250	3.60	1.25 V_o	1170
3	0.300	3.00	1.50 V_o	1690
4	0.350	2.57	1.75 V_o	2300
5	0.400	2.25	2.00 V_o	3000
6	0.180	5.00	0.90 V_o	600

(b) Variable area, constant volume.

Specimen No.	Diameter in.	Length in.	Surface Area $(in.)^2$	Load lb.
7	0.300	2.00	S_o	1690
8	0.275	2.375	1.1 S_o	1420
9	0.250	2.875	1.2 S_o	1170
10	0.200	4.50	1.5 S_o	750

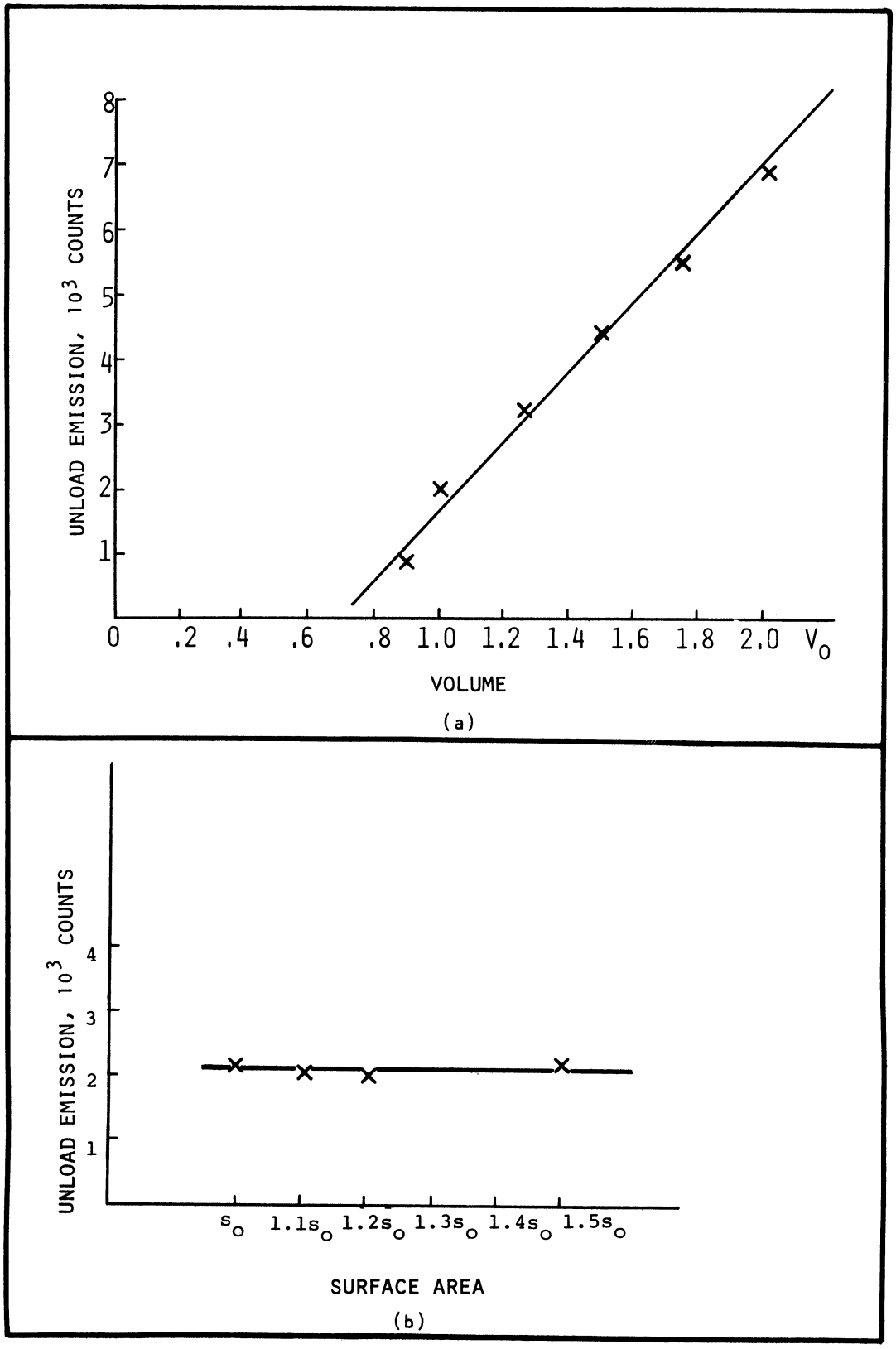

Figure 3.3 Effect of the Size of the Specimen on Unload Emission. (a) Constant Surface Area. (b) Constant Specimen Volume.

the material by a desired amount. Acoustic emission spectra were recorded from these specimens and the results are presented in Figure 3.4. Percent cold-work and hardness data are given in Table III.2.

3.2.4 Effect of Artificial Aging of 6061 Aluminum

Since the increase in the percent cold-work caused an increase in the hardness as well as increase in unload emission count, it was felt desirable to vary the hardness of a test material by a process other than cold-working and then to study its effect on the unload emission. Ten identical 6061 aluminum specimens were machined, and then solution treated by heating them to 975°F for four hours and water quenched. These specimens were then aged at 375°F for the number of hours indicated in Table III.3. Figure 3.5 shows how the unload emission count and the hardness changed with increasing amounts of aging time. It can be seen that unload emission count increases as the hardness of the material increases and vice-versa.

3.2.5 Effect of the Change in the Maximum Induced Stress

Figure 3.6 shows the variation of the unload emission count plotted against the maximum stress reached. Several different materials were investigated and in each case the specimen was loaded to a certain stress level and then unloaded. The same specimen was reloaded to a higher level and again unloaded. The process was continued for several values of maximum load. The unload emission count for all materials tested increases almost linearly up to a certain value of the maximum stress and then tends to remain constant.

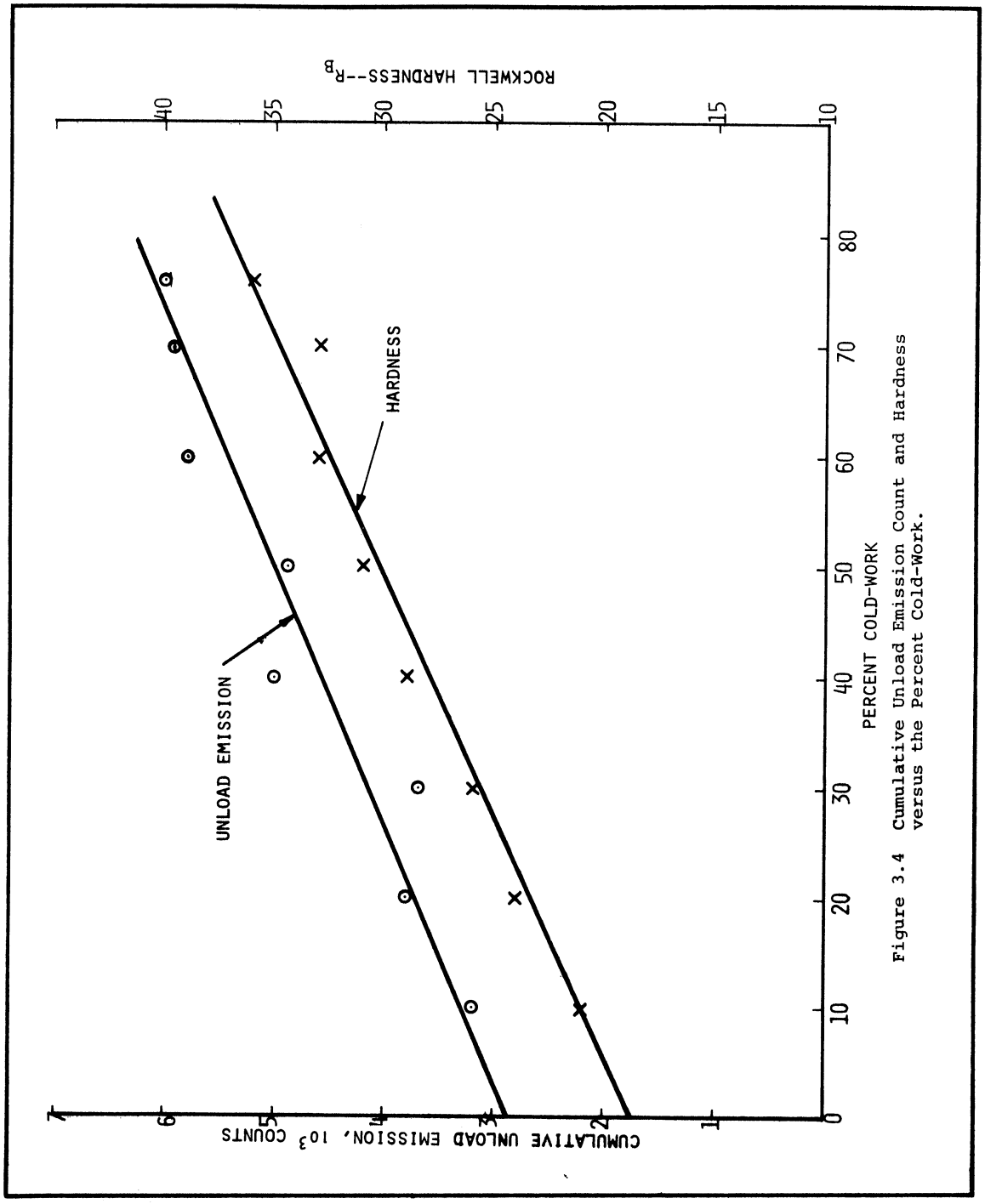

Figure 3.4 Cumulative Unload Emission Count and Hardness versus the Percent Cold-Work.

TABLE III.2

PERCENT COLD-WORK AND HARDNESS OF ALCOA 195 ALUMINUM SPECIMENS

Specimen No.	Percent Reduction in Area	Hardness R_B
CW-0	Annealed	18.0
CW-1	10	21.0
CW-2	20	24.0
CW-3	30	26.0
CW-4	40	29.0
CW-5	50	31.0
CW-6	60	33.0
CW-7	70	33.0
CW-8	76	36.0

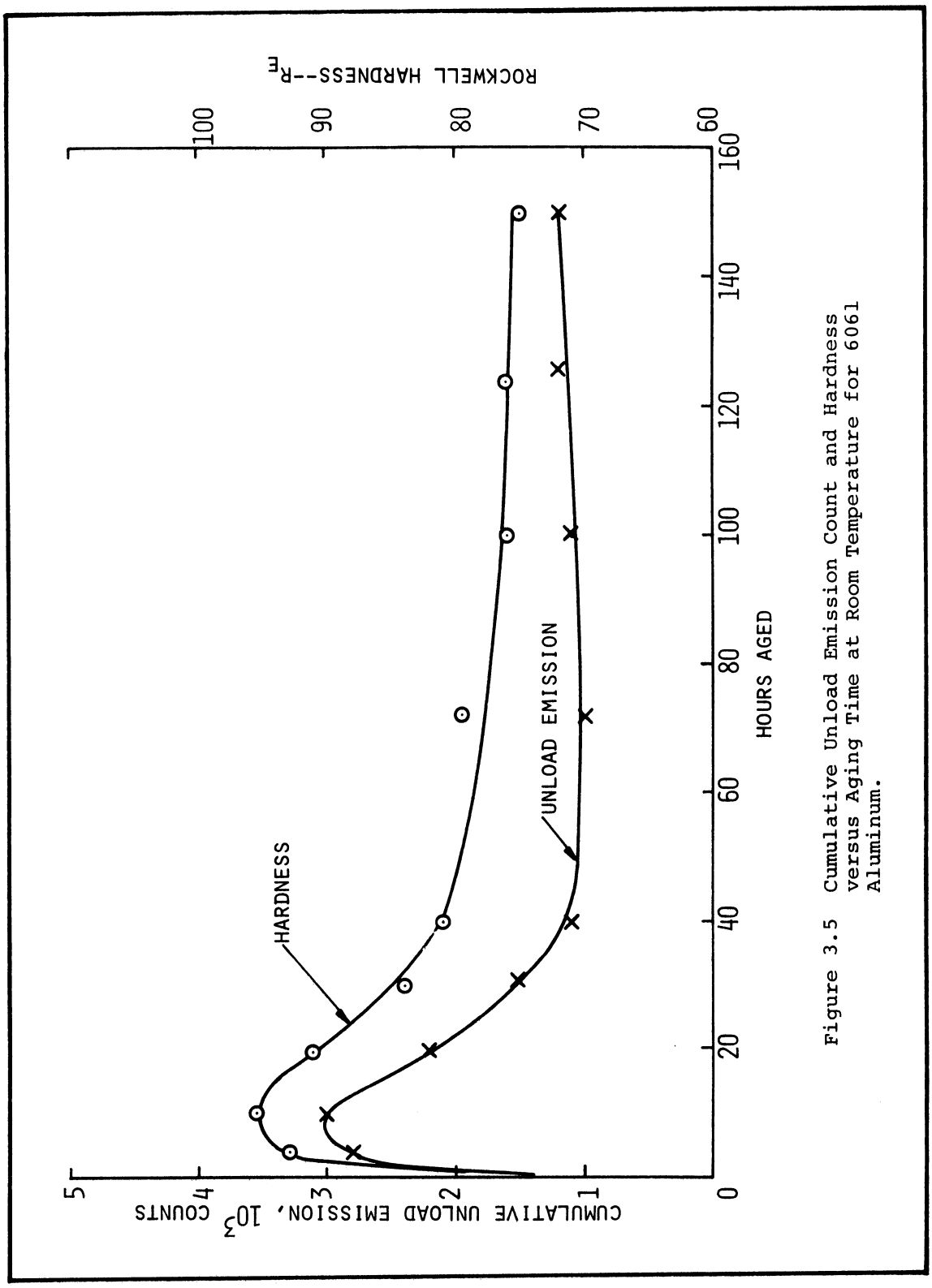

Figure 3.5 Cumulative Unload Emission Count and Hardness versus Aging Time at Room Temperature for 6061 Aluminum.

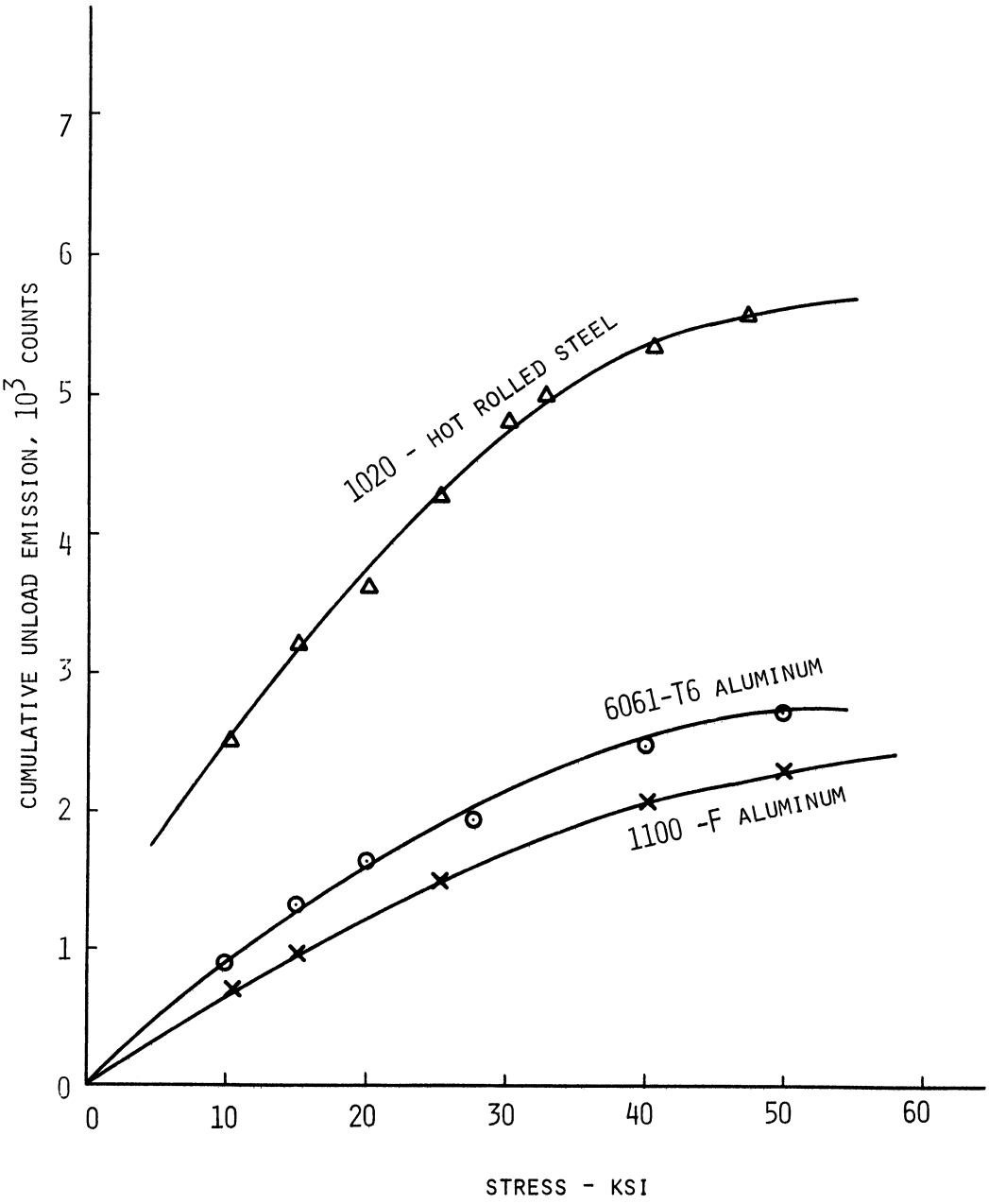

Figure 3.6 Cumulative Unload Emission Count, versus Maximum Applied Stress.

TABLE III.3

AGING TIME AND RESULTANT HARDNESS OF 6061 ALUMINUM

Specimen No.	Aging Time at 375°F	Hardness, R_E
1	0	62.0
2	4	93.0
3	10	95.5
4	20	91.0
5	30	84
6	40	81.0
7	72	79.5
8	100	76.0
9	125	76.0
10	150	75.0

TABLE III.4

UNLOAD EMISSION FOR SEVERAL MATERIALS

Material	Unload Emission Count
1020 H. R. Steel	12×10^3
302 Cold-drawn Stainless Steel	4.4×10^3
6061-T6 Aluminum	9.5×10^3
2024-T6 Aluminum	6.8×10^3

3.2.6 Comparative Value of the Unload Emission Count From Different Materials

In order to study the relative unload emission characteristics of several different materials, identical specimens were manufactured from the "as-received" bars of various materials. Each specimen was loaded to the maximum stress of 42,000 psi and then unloaded. Table III.4 shows the unload emission for the materials tested. In each case there was little or no emission during the loading cycle except for the first application of load. It can be seen that 1020 hot-rolled steel gives the maximum emission and stainless steel the least.

3.2.7 Effect of Aging Under An Applied Load

The effect of aging under an applied stress was studied in 2024 aluminum. Test specimens were solution treated at 975°F for four hours and water quenched. Since 2024 aluminum ages at room temperature, the specimens were loaded in the tensile testing machine within five minutes after quenching and allowed to age in the grips for 24 hours. Identical specimens were aged at room temperature outside of the grips for the same number of hours. Figure 3.7 shows the results. It can be seen that the unload emission behavior is different for the two cases. There is very little stress delay and there is a much larger emission activity just as the unloading begins in case of specimens aged within the grips. Similar behavior was observed when 1020 steel was strain aged under load. In this case the specimens were loaded beyond the yield point then aged for 20 hours at 180°F within the grips by using a heating unit which surrounded the specimen. Figure 3.8 shows the relative emission pattern of this specimen and an identical one aged outside the grips.

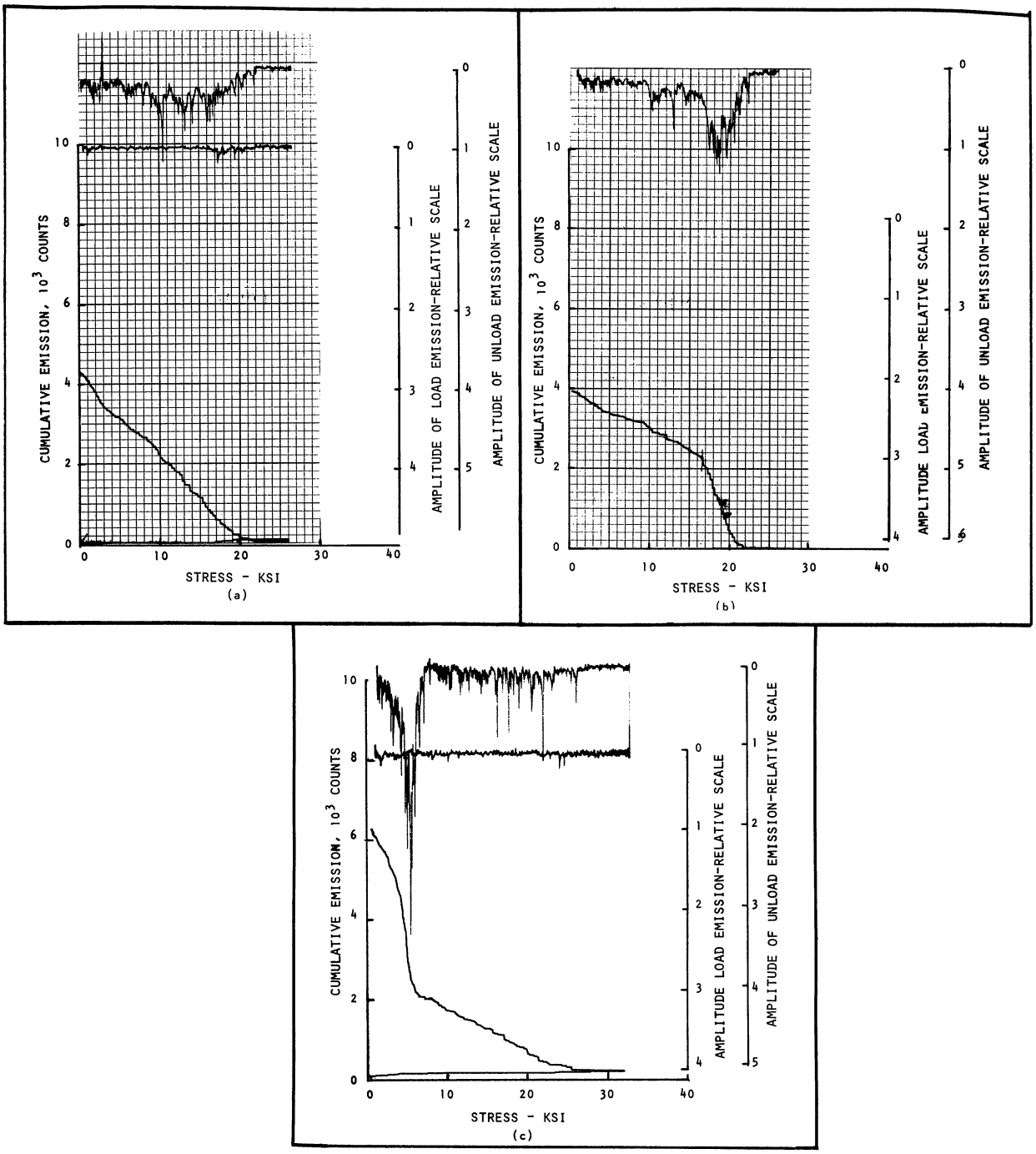

Figure 3.7 Effect of Strain-Aging on Unload Emission from 2024 Aluminum. a) Aged at Room Temperature for 116 Hours at Zero Stress, b) Aged at Room Temperature for 116 Hours at a Stress of 25 ksi, c) Aged at Room Temperature for 116 Hours After Unloading to 8 ksi.

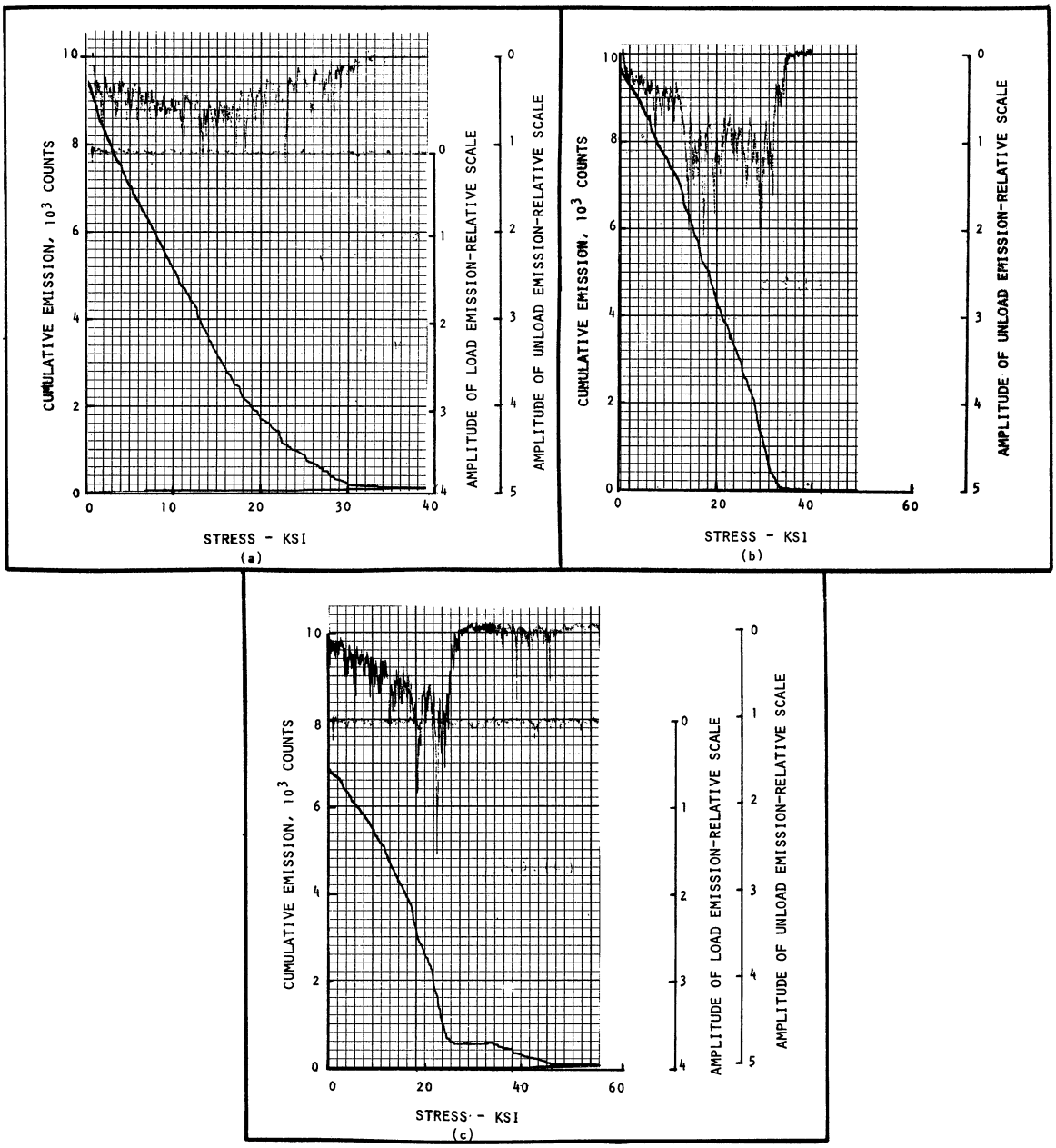

Figure 3.8 Effect of Strain-Aging on Unload Emission from 1020 Steel. a) Aged for 20 Hours at 180°F at Zero Stress, b) Aged at 180°F for 20 Hours at a Stress of 40 ksi, c) Aged at 180°F for 20 Hours After Unloading to 30 ksi.

Partly unloading the specimen and then aging it within the grips gives rise to an unload emission behavior identical to that of aging before unloading began.

3.2.8 Emission From Specimens Loaded in Compression

Several 1020 steel and 6061 aluminum specimens were loaded in compression. A typical emission spectrum obtained is presented in Figure 3.9. There is no significant difference in the unload emission between the tensile and compressive loading modes. No emission could be detected during the loading cycle at the values of threshold sensitivity that were used.

3.3 Load Emission

With the exception of the 1020 hot-rolled steel, all materials tested in their as-received and machined condition revealed that there is little or no emission when the specimens are loaded (see Figure 3.1). Although the exact processing history of the materials is not known, from the specified tempers and hardness data it can be deduced that in their as-received condition the aluminum bars were either precipitation hardened or cold drawn. All other materials tested were in the cold drawn condition.

3.3.1 Emission From 1020 Hot Rolled Steel

First loading of an as-received 1020 hot-rolled steel specimen gives rise to a large load emission (see Figure 3.10a), the onset of which is coincident with the yield drop. The emission continues through the yield elongation into the strain hardening region (see Figure 3.11 for definition of these terms) and then gradually diminishes.

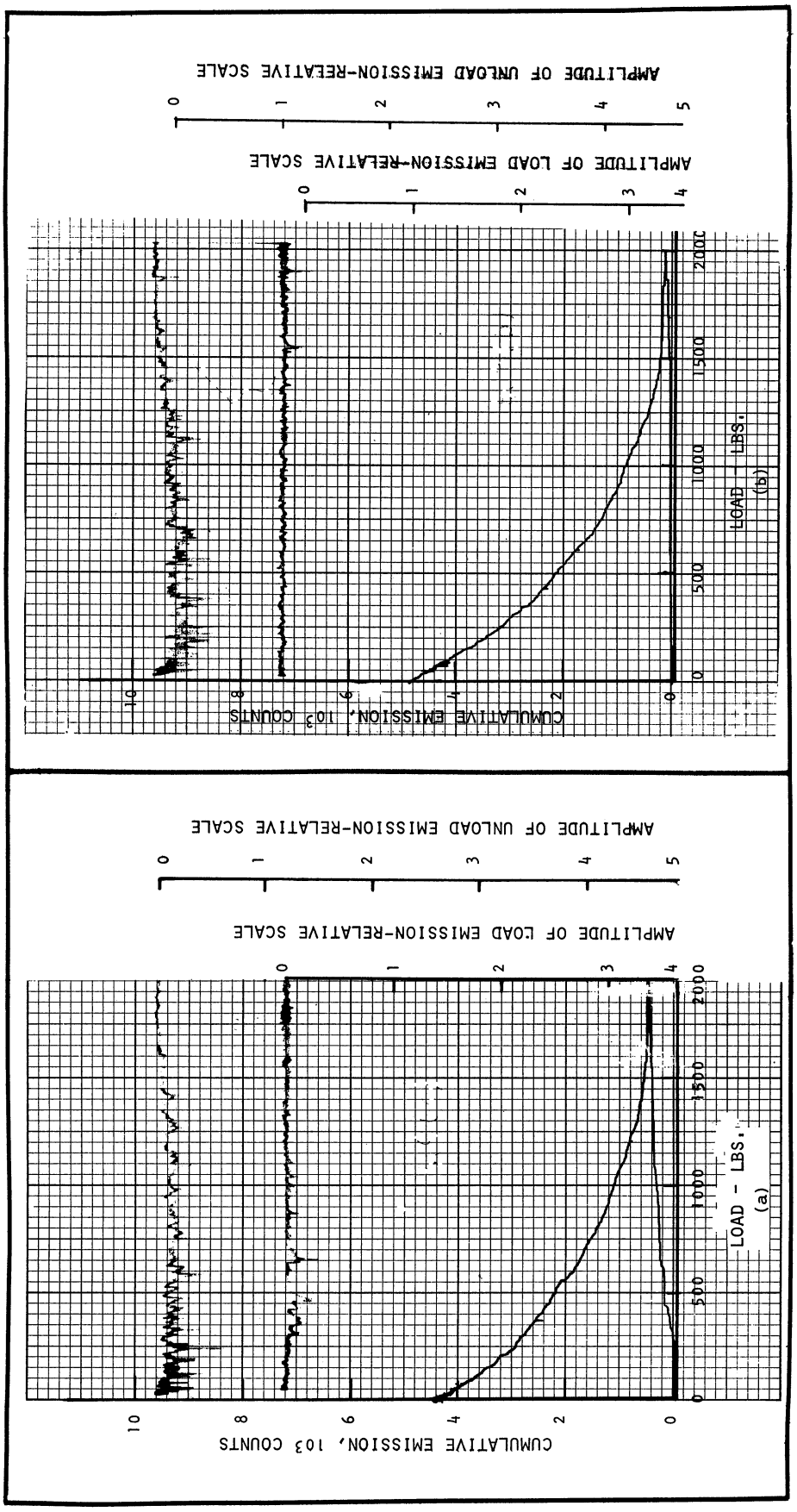

Figure 3.9 Emission Spectra for Compressive Loading. a) First Loading, b) Second Loading.

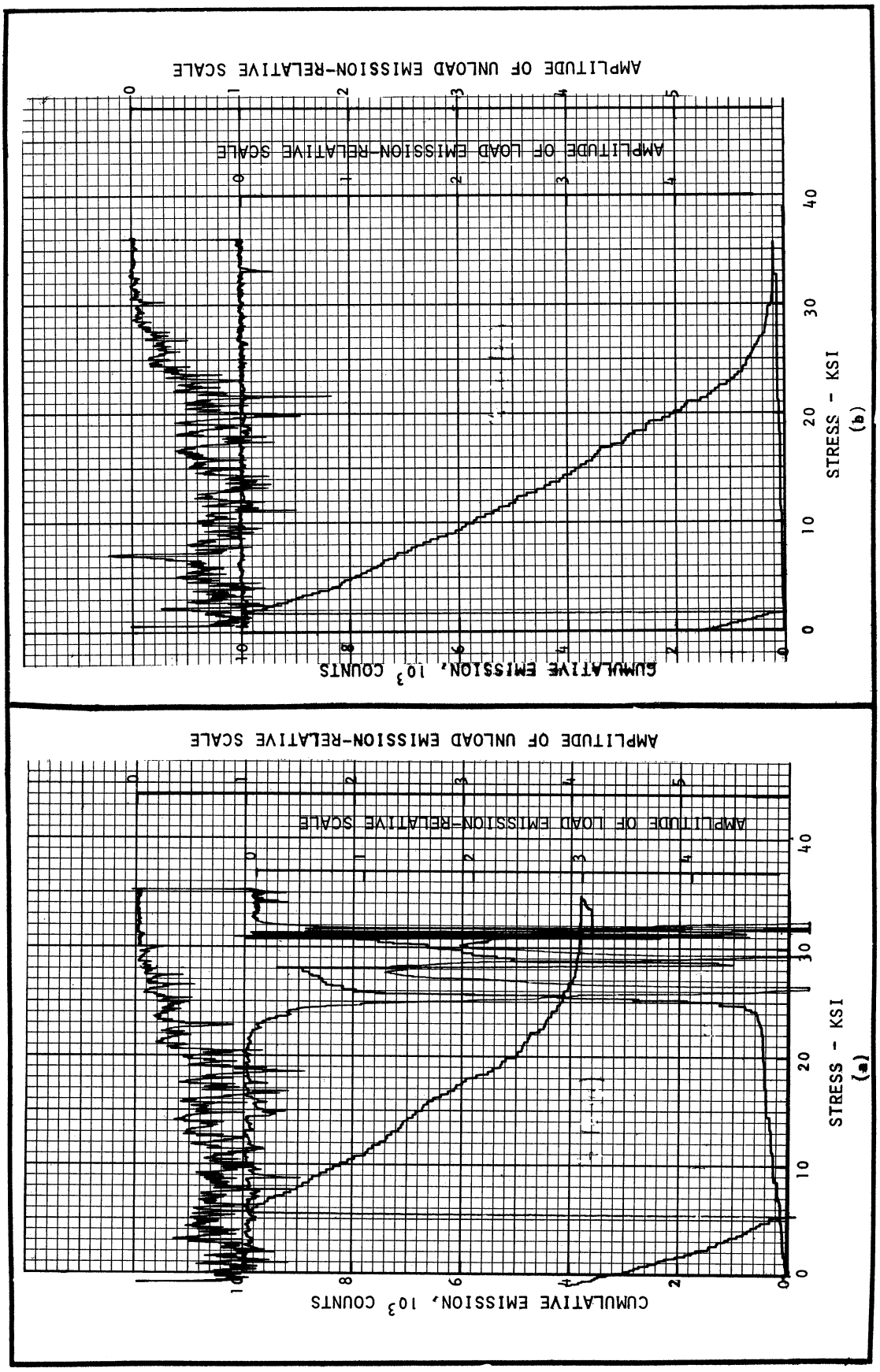

Figure 3.10 Emission from Annealed 1020 Steel. a) First Loading, b) Second Loading.

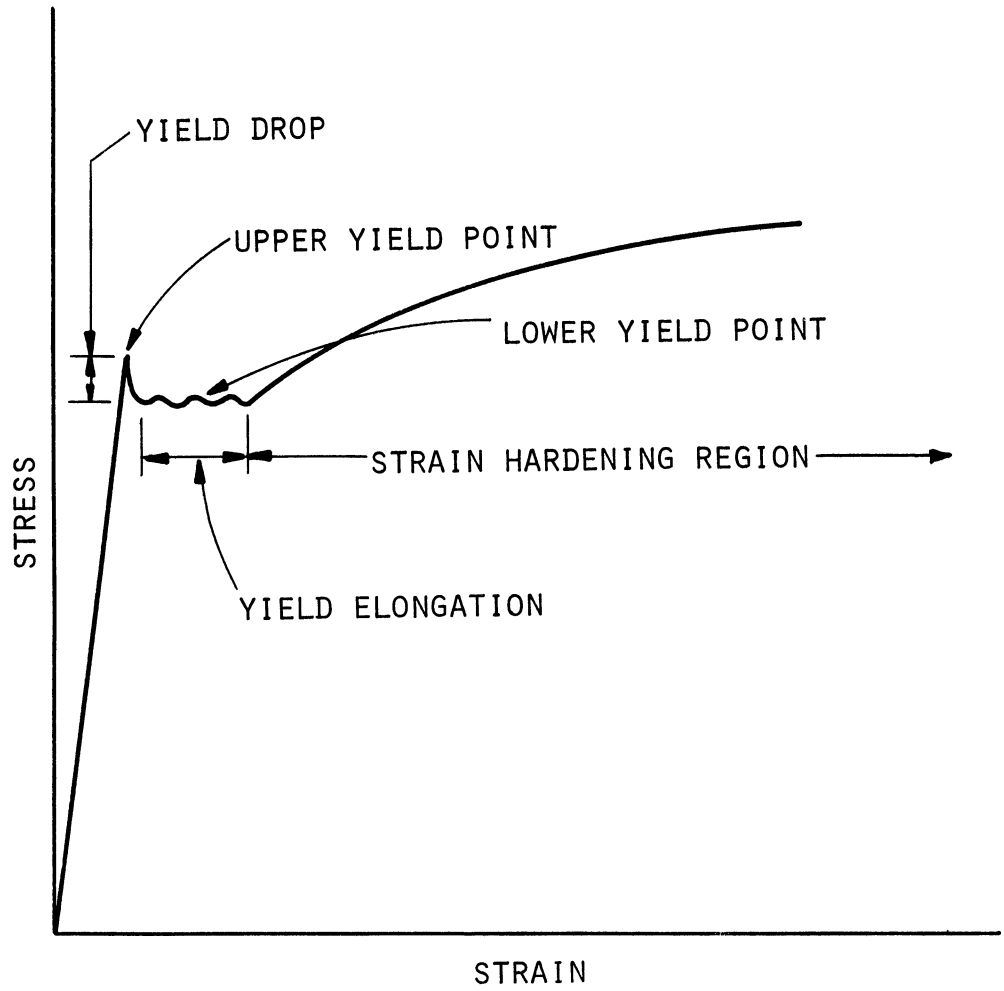

Figure 3.11 Stress-Strain Diagram for 1020-Annealed Steel (Schematic)

Further straining causes no more detectable emission. When a specimen, which has been loaded beyond the yield point in a manner just described, is unloaded and then reloaded, negligible emission activity is observed during reloading (Figure 3.10b). If, however, during the first loading the specimen is unloaded before the emitting process is completed, subsequent loading causes no detectable emission until the previous stress level is reached (Figure 3.12) at which point large load emission is observed. This phenomenon is known as the Kaiser effect.

3.3.2 Effect of Strain-Aging of 1020 Steel

Hot-rolled or annealed 1020 steel specimens show a sharp yield drop at the upper yield point during the first application of a load. The yield drop reappears at a slightly higher stress if, after some prestrain, the specimen is heated at 300°F for one or two hours. This phenomenon is called strain-aging. Specimens aged in this manner were loaded in the acoustic tensile machine. Figure 3.13 shows that there is virtually no emission during reloading even though the specimen is loaded to fracture.

3.3.3 Emission From 2024 Aluminum

As mentioned earlier, no emission activity could be detected from specimens machined from 2024-T6 aluminum during loading. However, when 2024 aluminum specimens were solution treated at 975°F for four hours and then quenched and tested very quickly, large load emission could be detected (see Figure 3.14). The load emission count decreases progressively as the time after quenching increases. Figure 3.15 shows

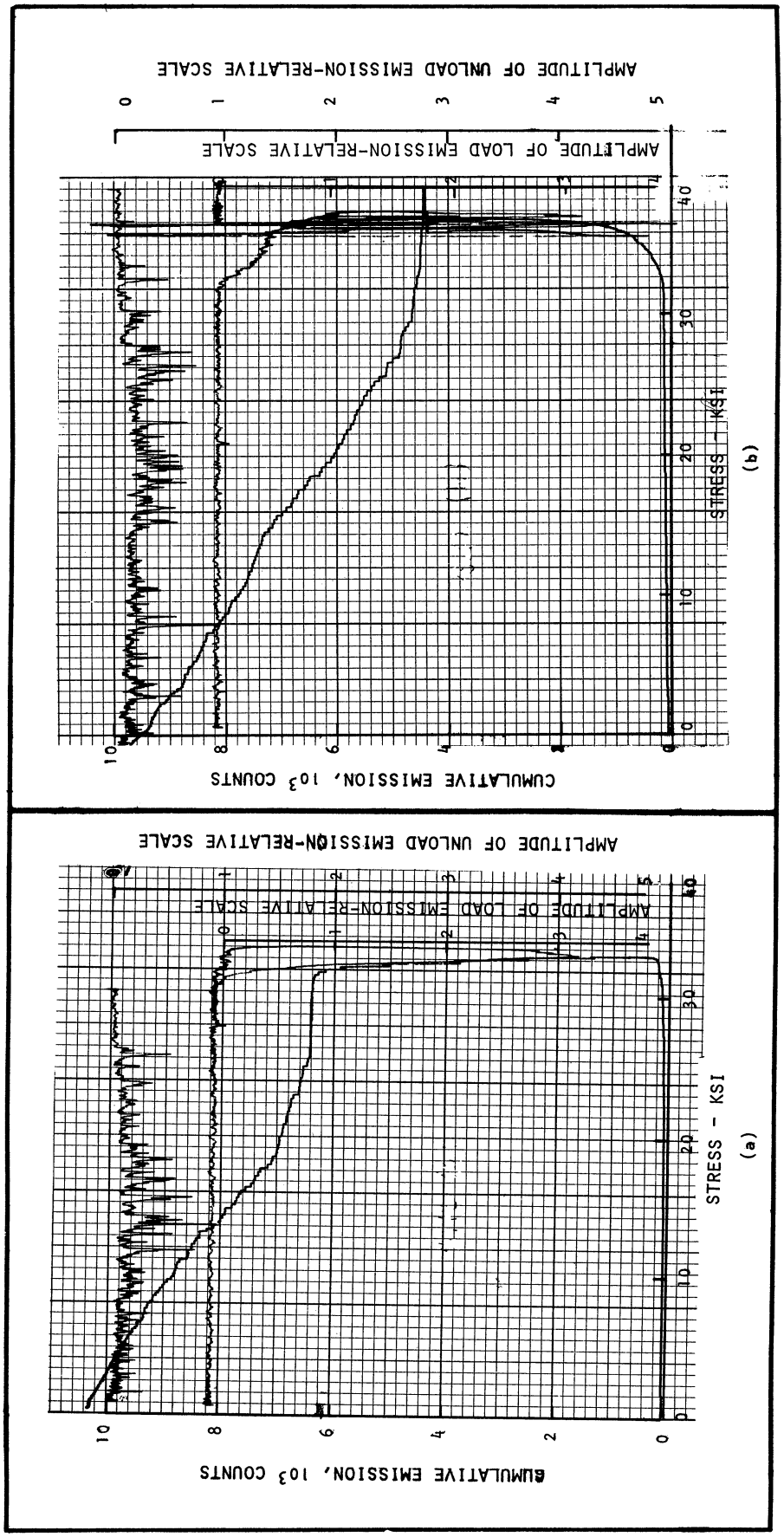

Figure 3.12 Kaiser Effect in Annealed 1020 Steel. (a) First Loading, (b) Second Loading.

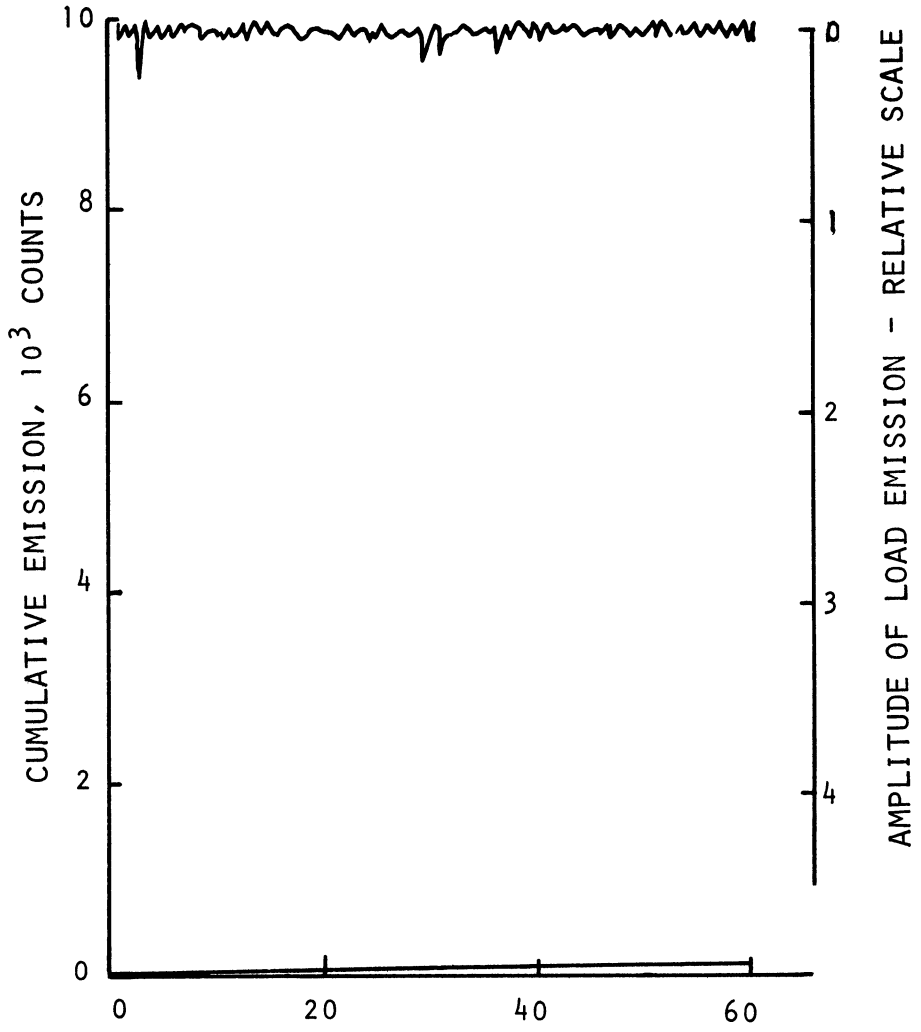

Figure 3.13 Emission from 1020 Steel, Strain Aged at 300°F for Two Hours (Specimen Fractured).

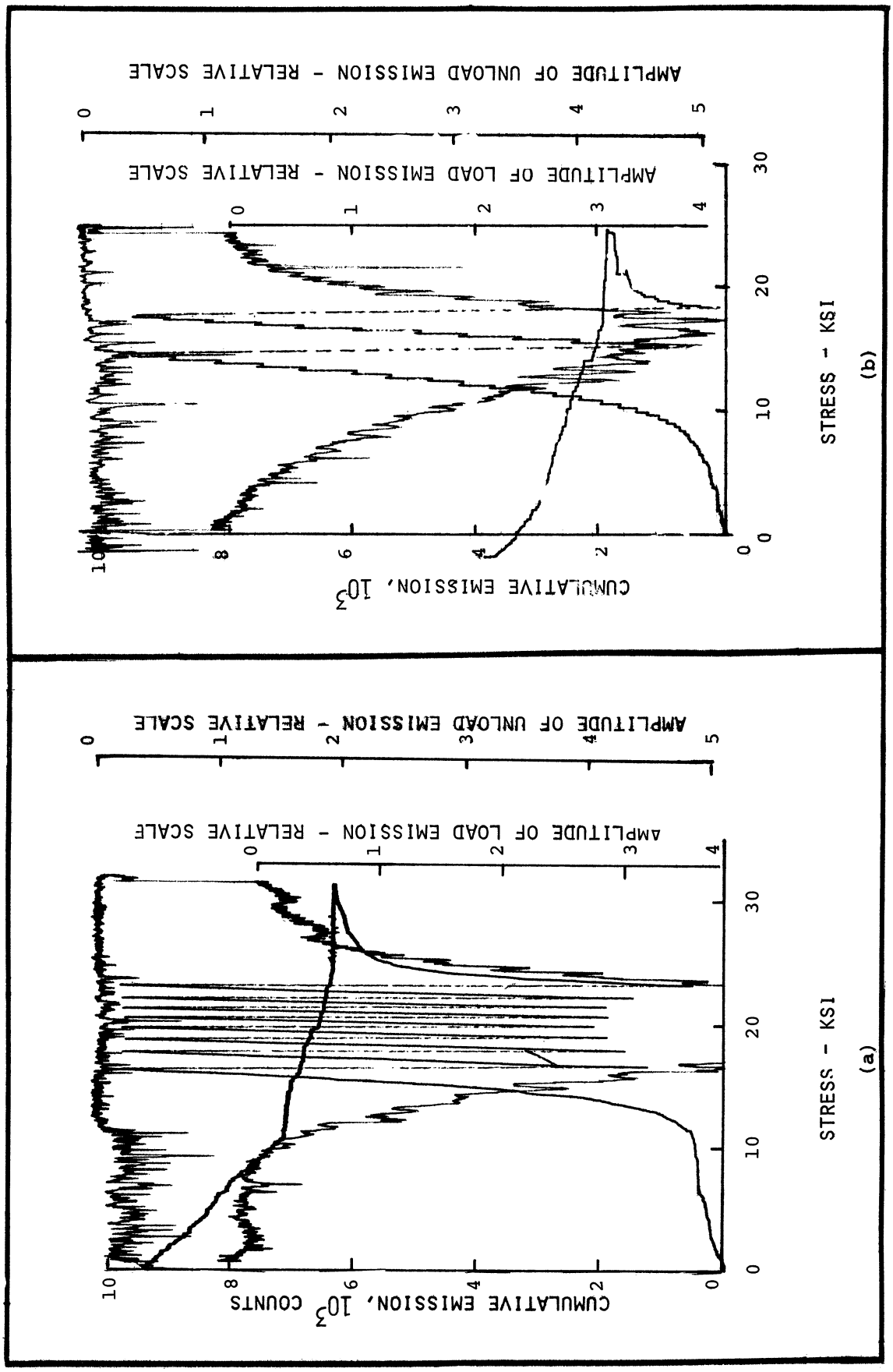

Figure 3.14 Emission from Solution-Treated 2024 Aluminum. a) 2.5 Minutes after Water Quenching, b) Six Minutes After Water Quenching.

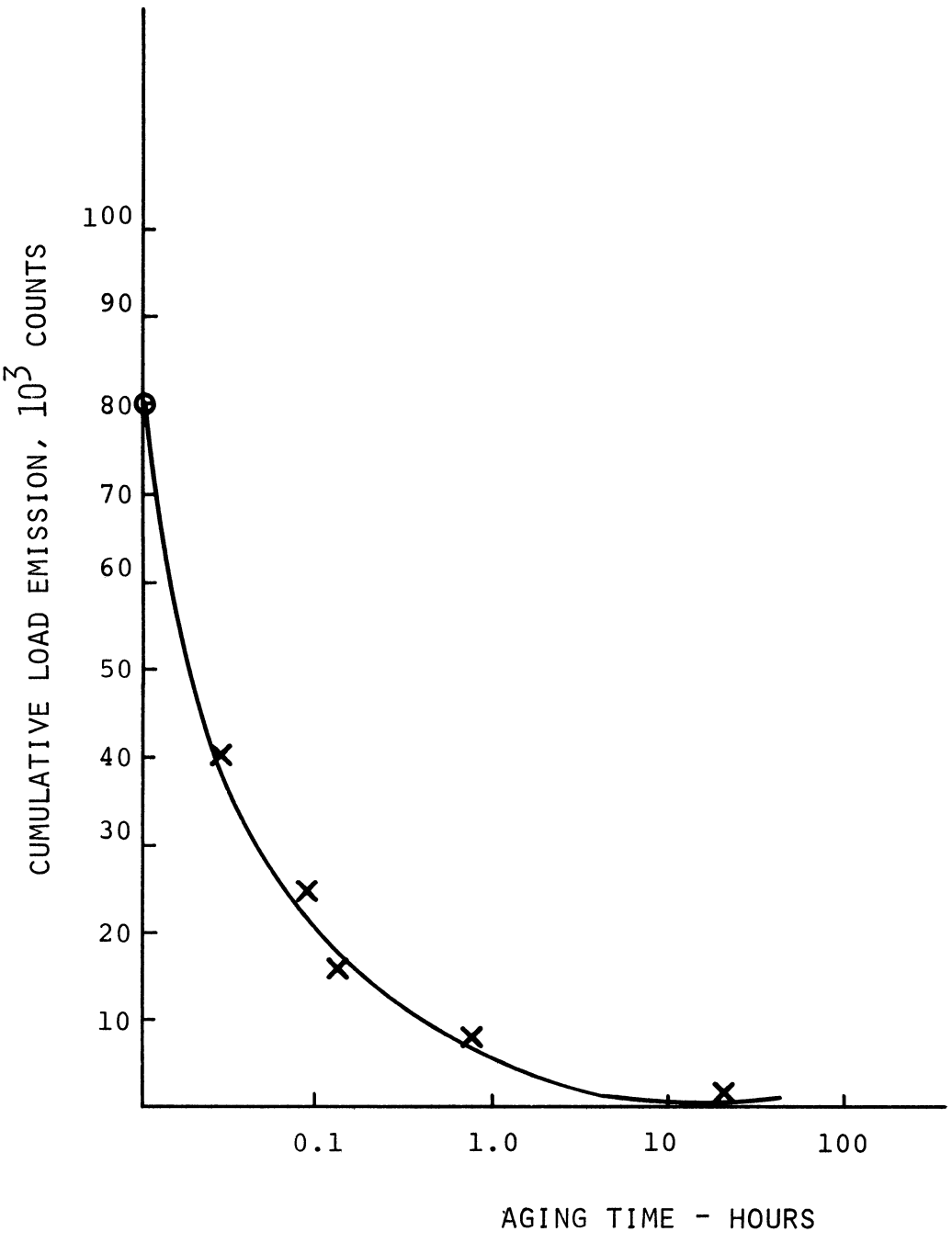

Figure 3.15 Cumulative Load Emission versus Aging Time at Room Temperature for 2024 Aluminum.

the plot of the load count as a function of time. It can be seen that after 20 or more hours after quenching the load count becomes negligibly small.

A series of tests was conducted to study the effect of microstructural variables associated with differences in the rate of cooling of 2024 aluminum. A number of specimens were heated to 975°F for four hours, some of these were air cooled, and others were cooled by leaving them inside the furnace and turning it off. When loaded in the acoustic machine, none of these specimens gave any detectable load emission (Figure 3.16).

The only process which showed any sign of bringing the load emission back was overaging of solution treated specimens. Specimens were aged at 600°F for 100 hours after solution treating and water quenching. When loaded these specimens gave a small amount of load emission (Figure 3.17).

3.3.4 Emission From Alcoa 195 Aluminum Alloy

Since 2024 aluminum ages at the room temperature, it was thought desirable to test grades of aluminum that do not age at room temperature. Alcoa 195 aluminum alloy was chosen for this purpose. In its solution treated and water quenched condition this alloy has essentially one phase, with most of the impurities in the solid solution.

Tests indicate that after solution treating at 975°F for four hours and water quenching, the behavior of this material is similar to that of 2024 (see Figures 3.14 and 3.18) aluminum described above except that the large load emission is detected even after the material has been held at room temperature for several days after quenching.

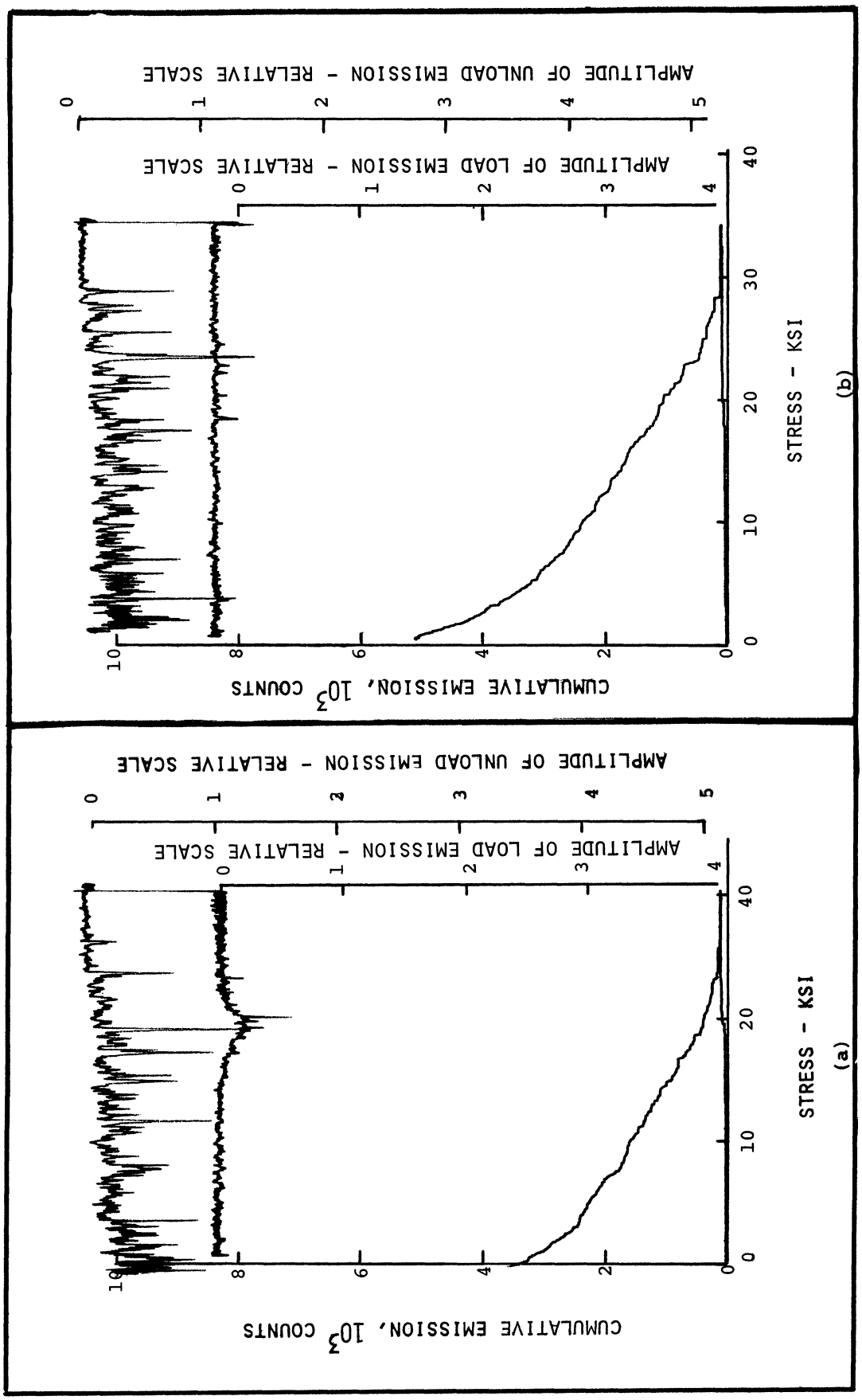

Figure 3.16 Effect of the Cooling Rate on the Emission from Solution-Treated 2024 Aluminum. a) Furnace Cooled, b) Air Cooled.

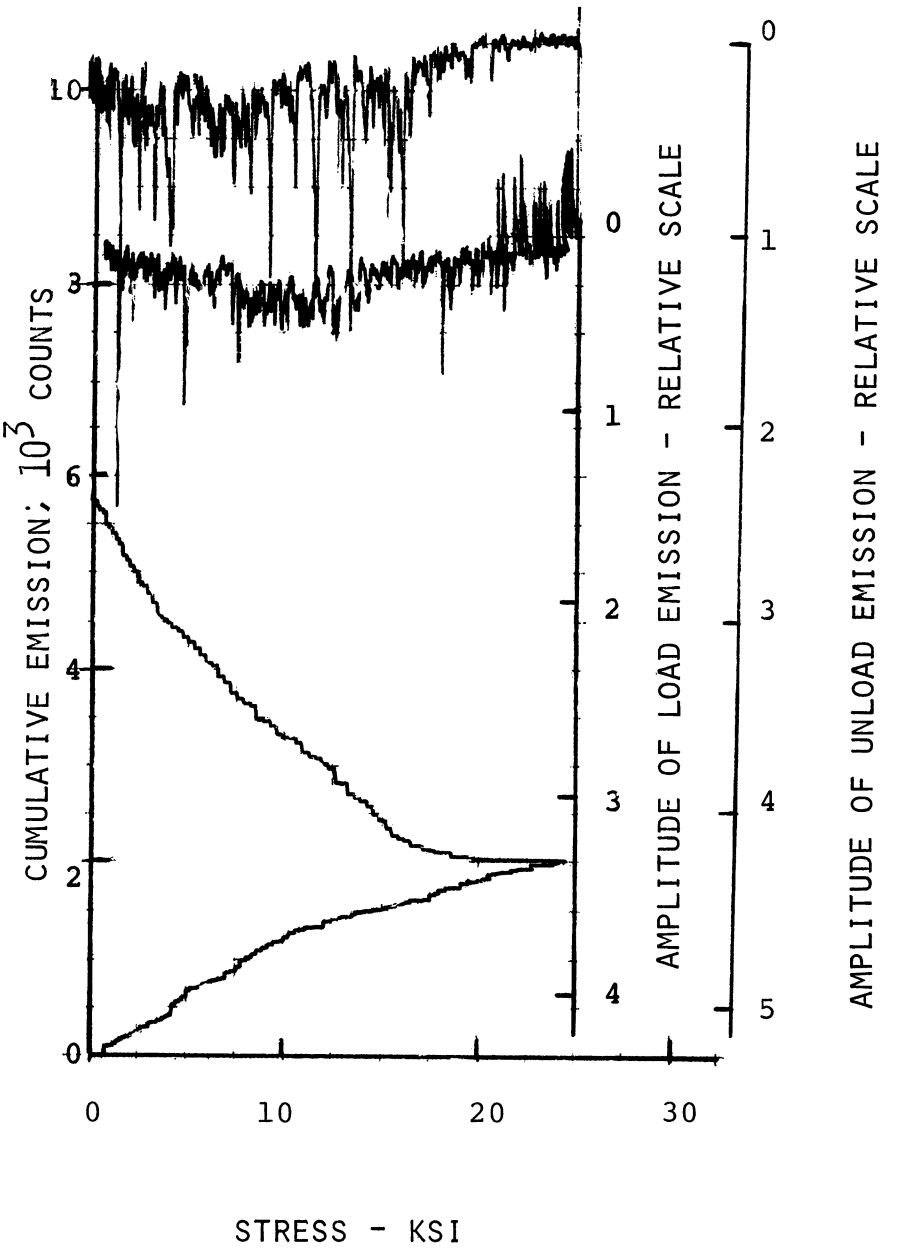

Figure 3.17 Emission from Overaged 2024 Aluminum. (Aged at 600°F for 100 Hours after Solution-Treating at 975°F for Four Hours).

The surface of some of these solution-treated and water-quenched specimens was removed by varying amounts either by machining or by etching (see Figure 3.18). In each case there was only a slight decrease in the load emission activity. The amount of surface removed does not seem to affect the emission behavior.

3.3.5 Load Emission From High Purity Aluminum

The experiments performed on 2024 steel and Alcoa 195 aluminum alloy indicate that the presence of the alloying elements drastically changes the load emission behavior. Hence, it was decided to test higher purity aluminum and study its load emission behavior. Three aluminum bars of 99.99 percent purity (composition given in Table II.1) were obtained from the Aluminum Company of America. From two of these bars standard specimens were machined. When one of these was tested for acoustic emission it gave no load emission. The second specimen was heated to 950°F for four hours and water quenched. Upon testing in the acoustic loading machine it was found to give a large amount of load emission only on the first loading. The same specimen was heated again to 950°F and this time air cooled. Once again there was load emission similar to that from water quenched specimens. Heating this specimen a third time, furnace cooling and testing shows no significant change in the emission spectra (see Figure 3.19). The third bar of the 99.99 percent purity aluminum was heated to 950°F for four hours and water quenched. It was then compressed in the longitudinal direction so that its initial length was reduced to three inches. Then it was compressed in the lateral direction until its length was three and one-half inches. It had an

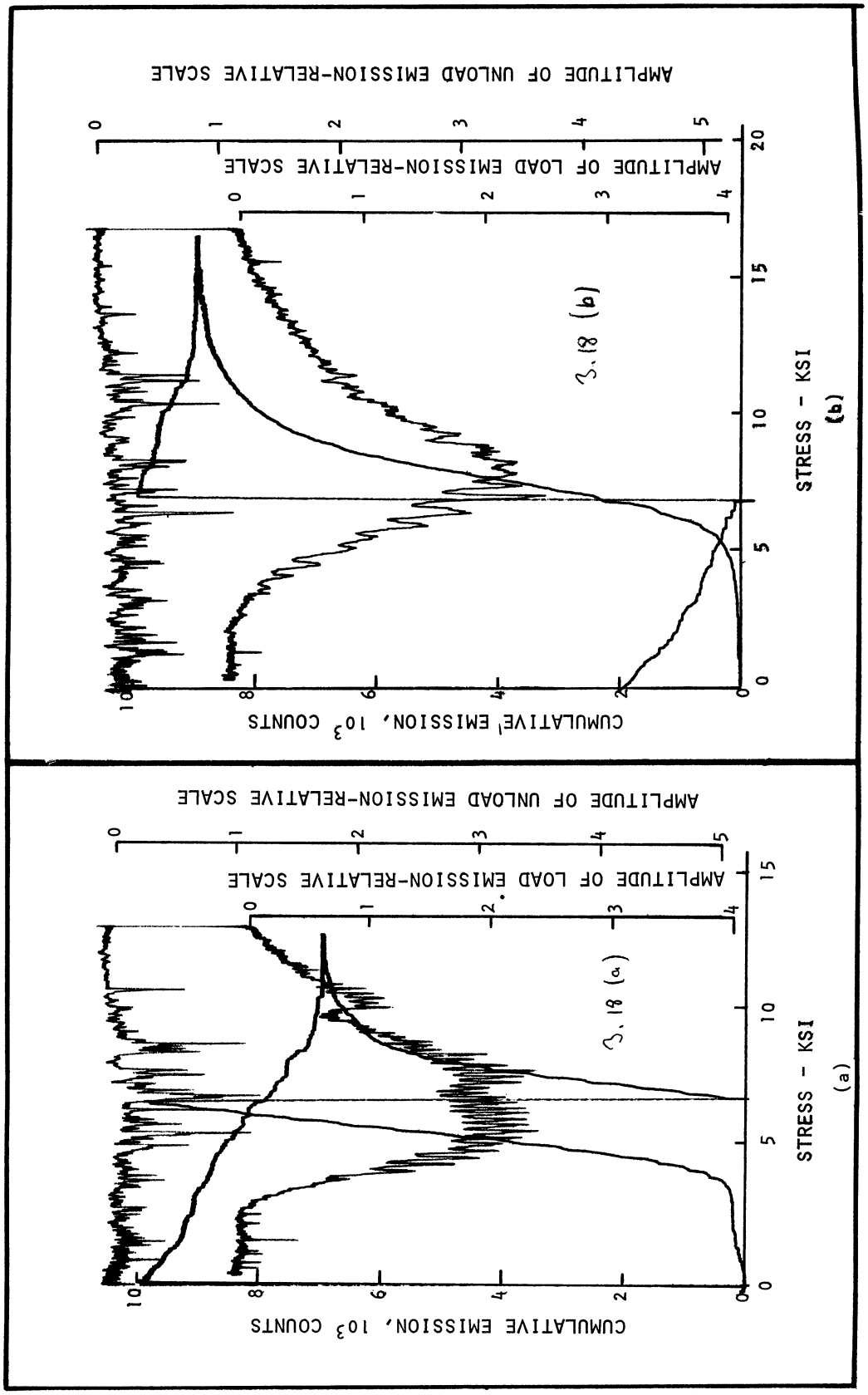

Figure 3.18 Emission from Solution-Treated Alcoa 195 Aluminum Alloy. a) Solution Treated at 975°F for 4 Hours and Water Quenched, b) Same Treatment as in (a), and Diameter Reduced by .003 Inch by Machining.

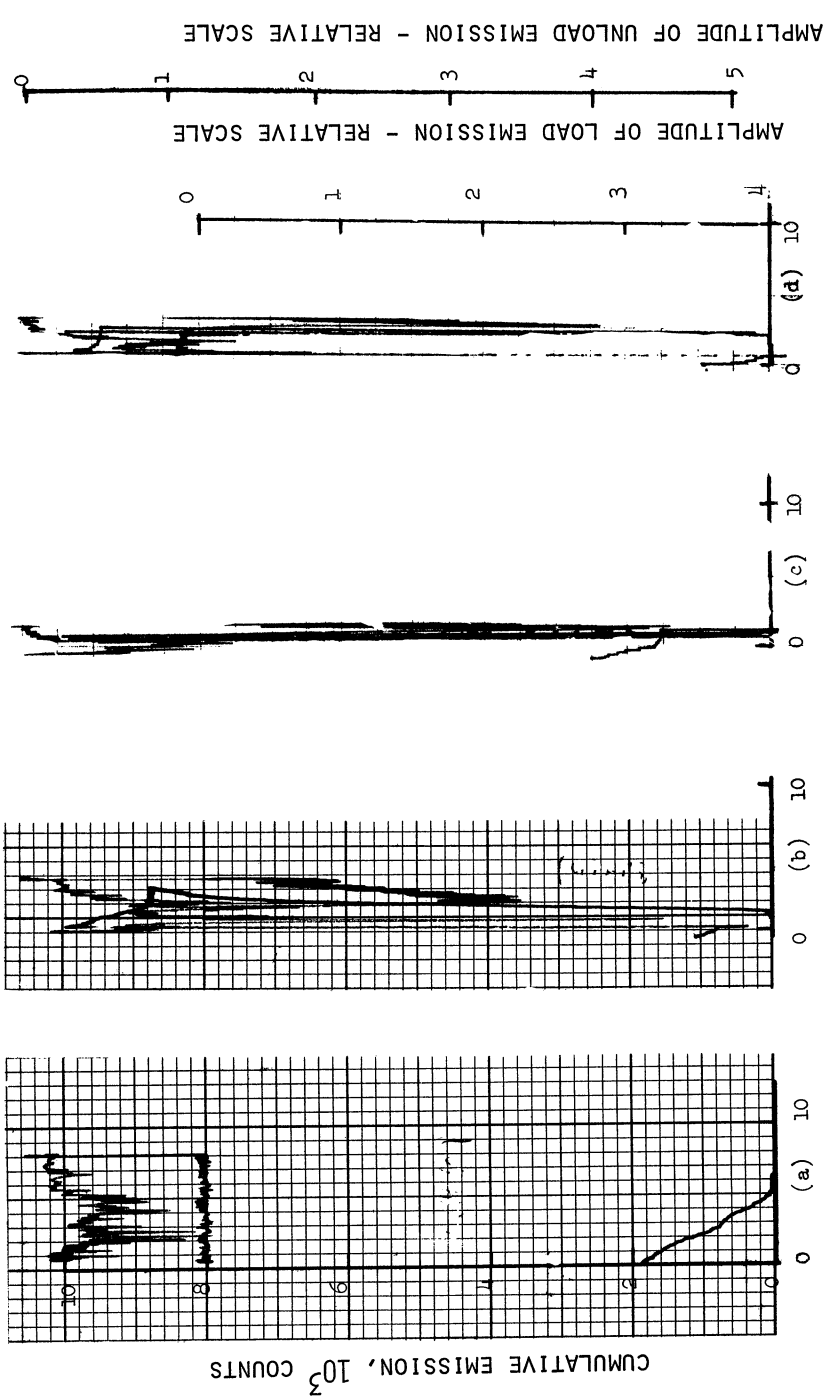

Figure 3.19 Emission from High-Purity (99.99%) Aluminum. a) As Received, b) Heated at 950°F for Four Hours and Water Quenched, c) Heated at 950°F for Four Hours and Air Cooled, d) Heated at 950°F for Four Hours and Furnace Cooled.

octagonal cross section at this stage. A specimen was then machined out of this bar and tested. As can be seen from Figure 3.20 very little load emission was detected from this specimen even for the large plastic deformation resulting from necking.

3.3.6 Load Emission From 1042 Steel

A 1042 cold drawn steel bar was purchased and specimens were manufactured from it. No load emission could be detected from these specimens in the as-received condition. It was then decided to study the effect of heating this material to 1550°F for three hours and water quenching so as to get martensite. Figure 3.21 shows the acoustic emission spectra obtained from such a test. There is a small amount of emission as the load is increased gradually, but at a stress of about 98,000 psi large emission activity is detected, this continues up to a stress of about 100,000 psi, at which the specimen breaks.

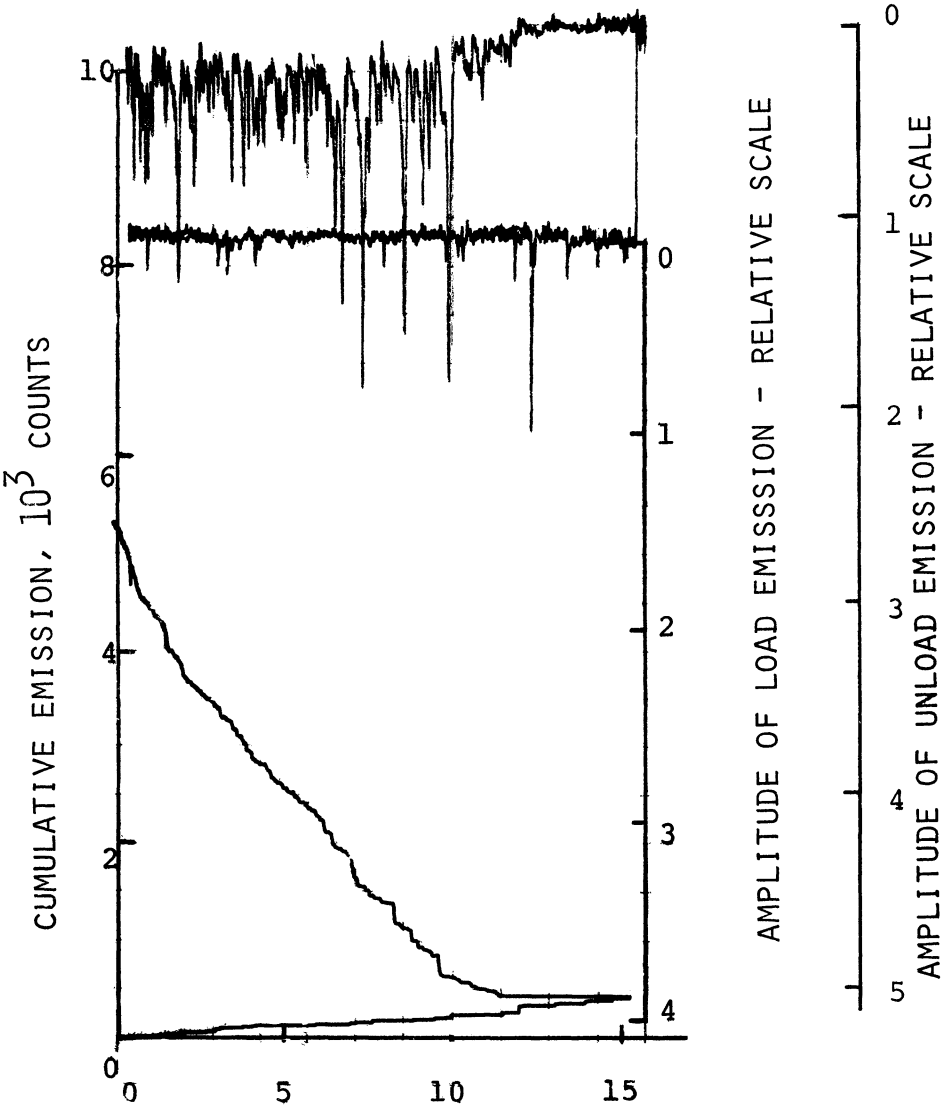

Figure 3.20 Emission from Cold-Worked High-Purity (99.99%) Aluminum.

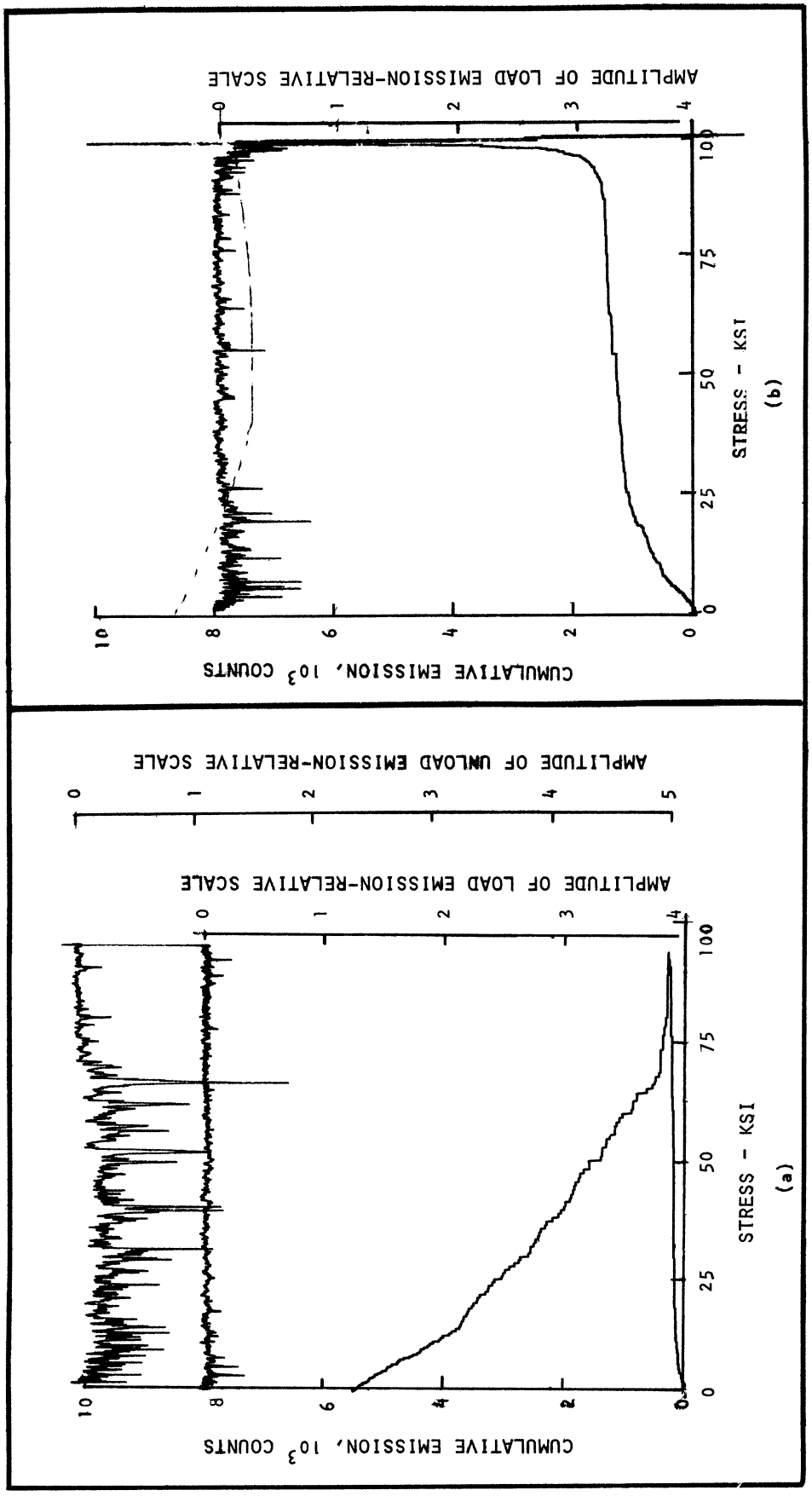

Figure 3.21 Emission from 1042 Steel. a) As Received, b) Heated at 1550°F for 3 Hours and Water Quenched Specimen Loaded to Fracture.

CHAPTER IV

DISCUSSION

4.1 Explanation of the X-Y Recorder Output Data

Definition of a few terms and a brief explanation of the form in which the data are presented on the X-Y recorder is desirable before a detailed discussion and interpretation of the results can be considered. For reasons of uniformity, an attempt has been made to use the same nomenclature as used by Kerawalla[7] and Mitchell.[8] Figure 4.1 is an actual X-Y recorder output, representing the emission behavior of a 2024 aluminum specimen for two consecutive load unload cycles. The abscissa is the applied stress and the ordinate is the cumulative emission count and the amplitude of the emitted pulses. The cumulative emission count variable has a zero at the bottom of the plot and increases upwards. The loading part of this curve is labelled as (1) and the the unloading part as (2). When the total number of counts reaches the 10,000 mark, the pen shifts down to the zero position and starts over again. Hence each spike on the emission count curve represents 10,000 counts. Figure 4.2 shows schematically the appearance of the same data if the pen were not to restart at zero after every 10,000 counts. The absence of any such peak in the second cycle of emission count data indicates that cumulative emission in the loading and unloading operation is less than 10,000 counts. Curve 3 is the plot of the amplitude of load-emission versus the applied stress; its zero starts about four inches above the zero of the count curve and increases downwards. Finally, curve 4 is the amplitude of unload emission plotted

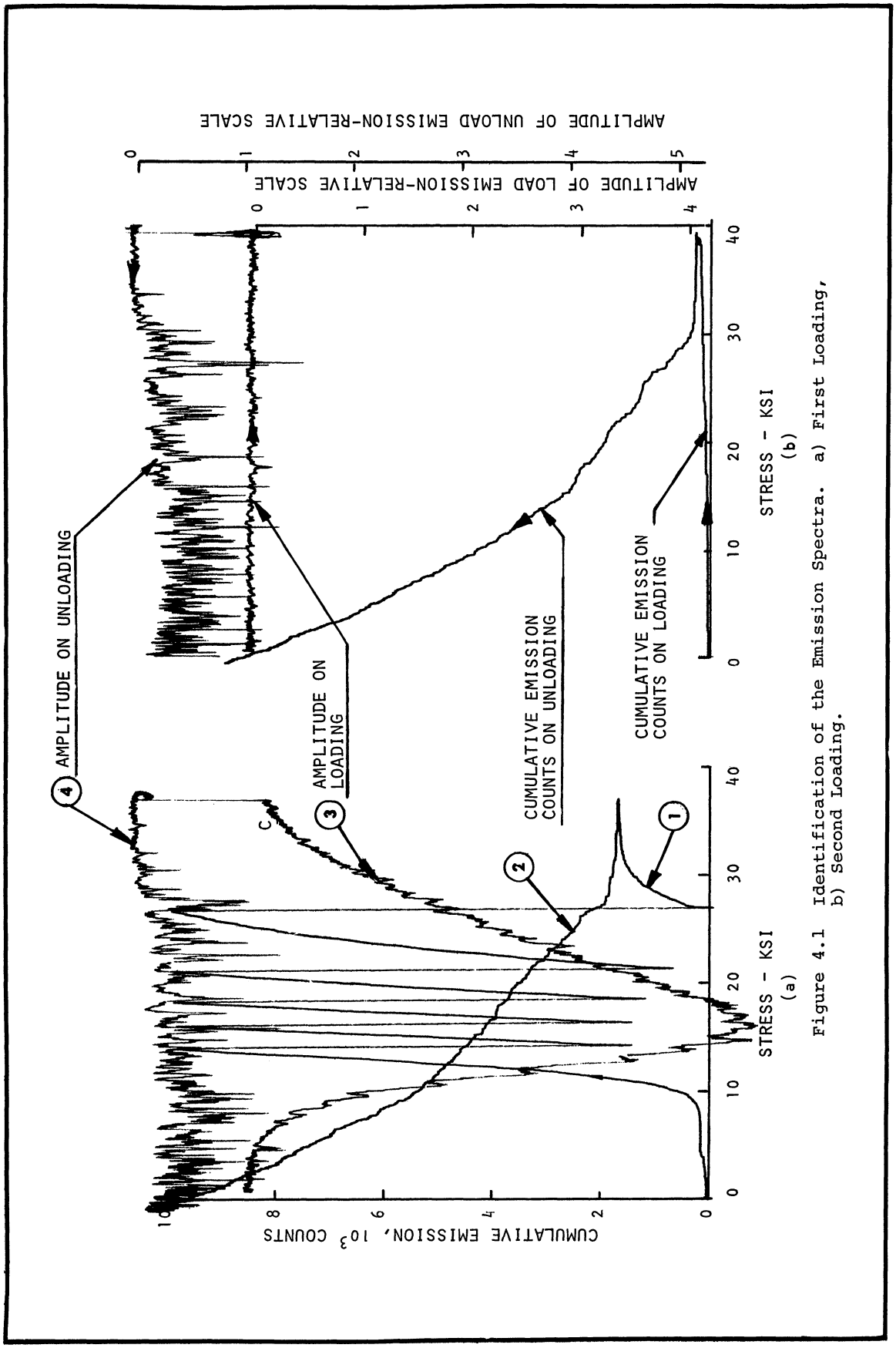

Figure 4.1 Identification of the Emission Spectra. a) First Loading, b) Second Loading.

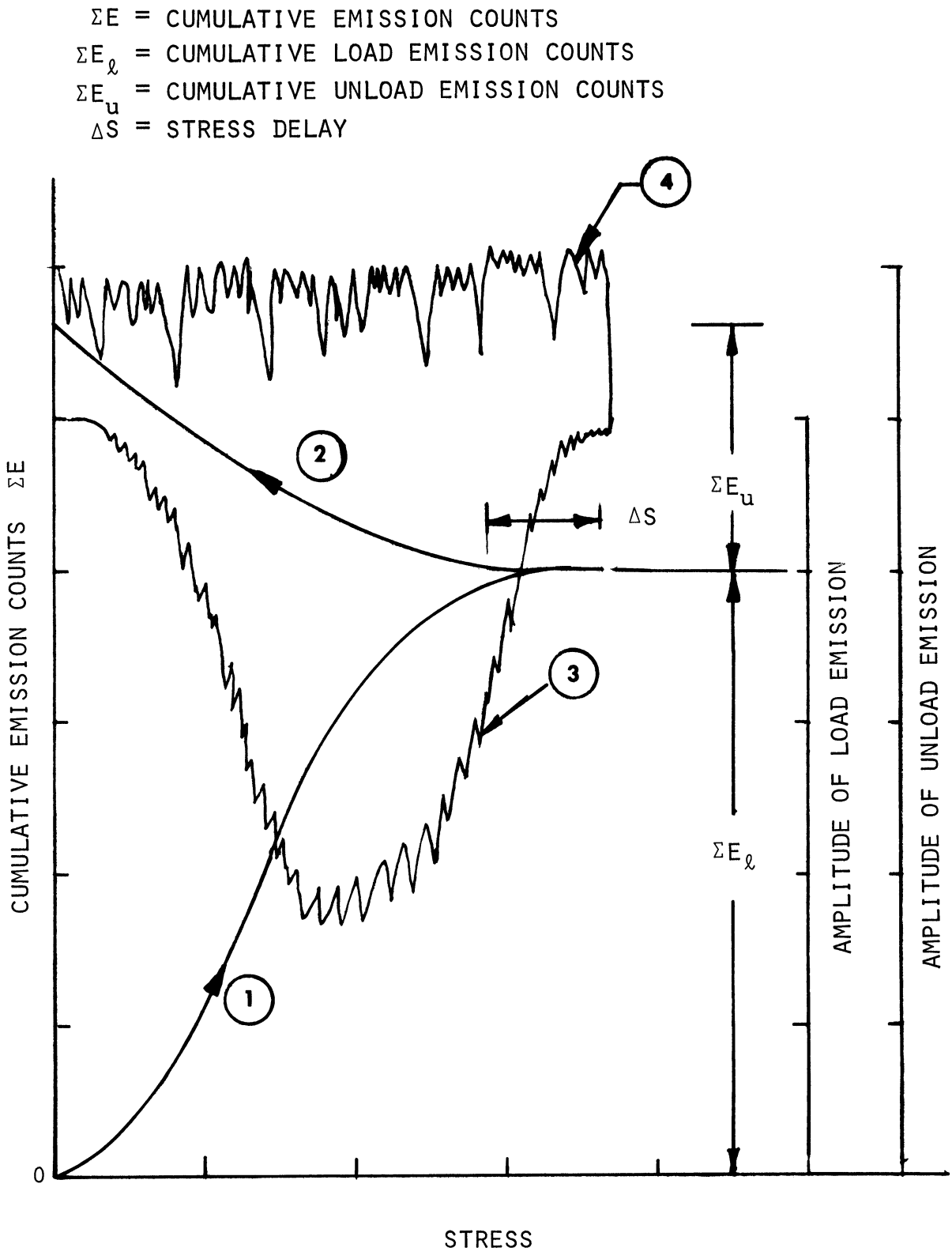

Figure 4.2 Emission Spectra (Schematic).

as a function of the stress. The zero of this curve is shifted above that of curve 3 by about an inch. Curves 1, 2, 3, and 4 have been clearly labeled in Figure 4.1 and 4.2 and the same nomenclature applies to all the X-Y recorder outputs presented in this report.

4.2 Terminology

The cumulative emission count which is designated as ΣE is the sum of ΣE_ℓ, the cumulative emission count during loading and ΣE_u the cumulative emission count during unloading. When unloading begins, there is a period of no emission activity; this is measured in terms of the amount of unload and is designated as Δs as shown in Figure 4.2.

4.3 Load Emission

4.3.1 The Model

Well annealed materials contain about 10^6 dislocations per square centimeter, distributed on a three-dimensional network known as the Frank Network.[11] Prolonged thermal treatment at elevated temperatures allows dislocations to move into a low energy configuration. Mott[12] showed that it is geometrically possible for three dislocations to meet in a point and form a node such that their Burgers vectors add up to zero. A random array of dislocations thus reduces to a rather stable three-dimensional network as shown in Figure 4.3. Network lengths such as AB are further pinned down by impurity atoms or precipitates. It is assumed that the pinning due to the nodes of the network and hard precipitates is so strong that no break-away of dislocation segments occurs under the action of applied stress. Dislocations may, however,

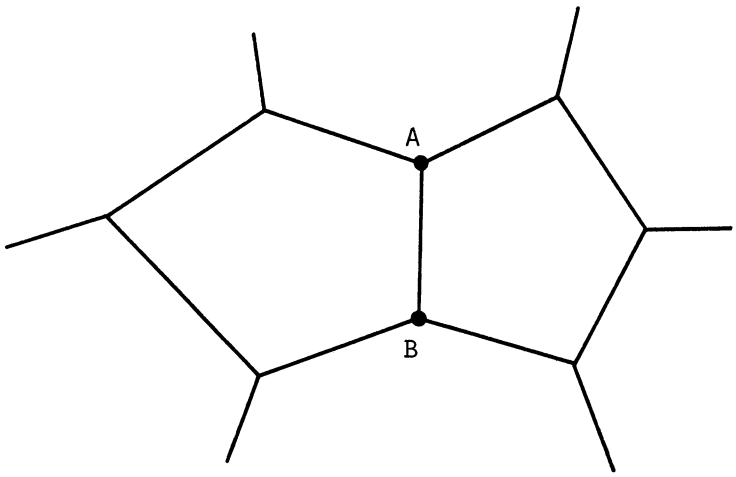

Figure 4.3 Frank Network.

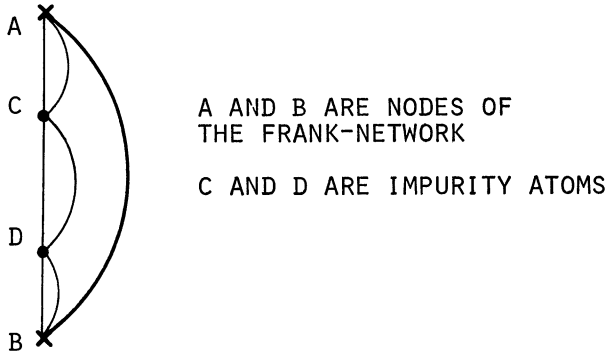

Figure 4.4 Bowing of Frank-Network
Due to Applied Stress.

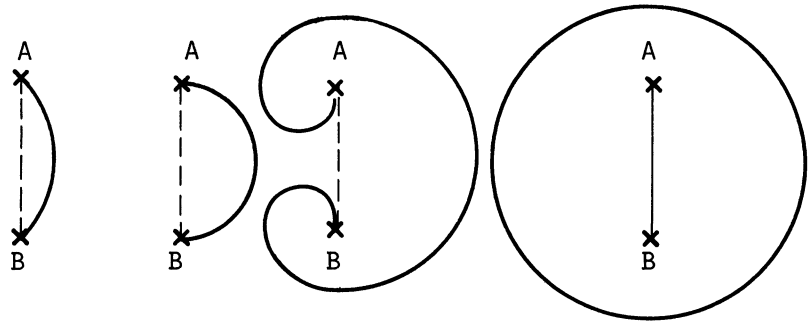

Figure 4.5 Operation of Frank-Read Sources.

break away from the impurity atoms as suggested by Cottrell.[13] It is known that crystals smaller than a few microns (whiskers) are almost free of dislocations; this suggests that smaller networks are unstable and grow rapidly by diffusion at high temperatures.[14] Hence, the network length should be of the order of a few microns; this belief has been supported by experimental evidence also.

Observations of thin films by electron microscopy[16] show that in most cold worked metals a three dimensional network of dislocations is developed. This is analogous to the Frank network but on a much smaller scale. This smaller network is also stable at room temperature but at elevated temperatures dislocations tend to reduce their total length and rearrange themselves to form a larger network.

When an external applied stress is increased, a dislocation line such as AB which lies in the slip plane has its subsections AC, CD, etc. (See Figure 4.4) bowed out and these continue to bow out until the break-away stress is reached at which point the dislocation frees itself from the relatively weak pinning of the impurity atoms. Further increase in the applied stress causes the dislocation length between points A and B to bow out as a whole. Points A and B are immobile because the segments of the dislocation network beyond A and B are out of the slip plane, hence the dislocation segment AB acts as a doubly pinned Frank-Read[17] source. Such a model has been used by Granato and Lucke[18] for developing a theory of dislocation damping.

The operation of a Frank-Read source is as follows:
When the material is stressed to cause slip, the dislocation line AB bows out successively as shown in Figure 4.5(a) to (d). A complete loop is generated and the line AB is formed again. It can be shown that the line AB bows out to a semi-circular shape when the shear stress attains a critical value given by the equation

$$\tau_{cr} = \frac{Gb}{\ell} \qquad (4.1)$$

τ_{cr} = Critical Shear Stress (newton/meter^2)
G = Shear Modulus (newton/meter^2)
b = Burgers Vector (cm.)
ℓ = Length of the dislocation line (cm.)

Further expansion of this line takes place without requiring any additional stress. The critical shear stress τ_{cr} is inversely proportional to the length, ℓ ; hence, the longer lengths will start to operate at lower stresses than the shorter ones.
A Frank-Read source is capable of generating an infinite series of dislocation loops. These loops keep on expanding until they are blocked by an obstacle such as the grain boundary, impurity particles, sessile dislocations, etc. The piled-up dislocations exert a back stress on the source, the magnitude of which depends upon the number of dislocations in a pileup. The source ceases to operate when the stress field around the pileup is such that the stress at the source falls below the critical value required for its operation.

A large number of theoretical and experimental studies have supported the above mentioned dislocation processes, and these processes have been used to explain various phenomena related to the mechanical behavior of metals. It is therefore assumed that such mechanisms are valid, and the following model explaining the acoustic emission behavior is proposed.

When a metal containing dislocations has Frank-Read sources greater than a certain critical length, detectable pulses are generated when an external applied stress activates them. The critical source length depends upon the sensitivity of the detection system used. Unfortunately, the techniques and the nature of the dislocation processes involved do not allow a very rigorous quantitative analysis; hence, the following calculations are presented to illustrate the procedure for making an order of magnitude estimate of the critical source length that is capable of producing detectable emissions.

4.3.2 Minimum Detectable Strain

The trigger level of the counter was set such that the smallest voltage peak, measured at the input of the preamplifier, that could trigger the counter was 4 microvolts.

The piezoelectric stress constant, g_{33}, for the PZT-5 crystal which is used as the detector, is 24.4×10^{-3} volt-meter/Newton and is defined as

$$g_{33} = \frac{\text{Volts per unit length of the crystal}}{\text{Stress, newton/meter}^2}$$

or

$$\text{Stress} \quad = \quad \frac{\text{Volts per unit length}}{g_{33}}$$

$$(\text{newton/meter}^2)$$

Length of the detector used = 25.4×10^{-4} meter

Minimum detectable voltage = 4 microvolts

Hence the minimum detectable stress = $\frac{4 \times 10^{-6}}{25.4 \times 10^{-4}} \times \frac{1}{24.4 \times 10^{-3}}$

$$\sigma_{min} = 0.0625 \text{ Newton/meter}^2$$

The strain in the material that results from this stress

$$\epsilon_{min} = \frac{0.0625}{E}$$

where E is the elastic modulus of the material of which the transducer is made. Substituting the value of E for PZT-5 crystal as 5.85×10^{10} Newtons/meter^2 we have the minimum detectable strain

$$\epsilon_{min} = \frac{.0625}{5.85 \times 10^{10}}$$

$$\simeq \quad 10^{-12}$$

In order to produce a detectable sound pulse the mechanism must account for the above minimum strain.

4.3.3 Number of Dislocations in a Pileup That Stops the Source

The stress field around a pileup containing n dislocations of like sign is given by

$$\tau_b = \frac{n\,Gb}{2\pi D} \qquad (4.2)$$

where

τ_b = back stress of the pileup acting to repel the last dislocation that forms, (newton/meter^2)

n = number of dislocations in the pileup

b = Burgers Vector, (cm)

D = average glide distance, (cm)

The source stops when this stress equals the critical value τ_{cr} given by the Equation (4.1).

Equating τ_b to τ_{cr} we get

$$\frac{n\ Gb}{2\pi D} = \frac{Gb}{\ell}$$

hence

$$n = 2\pi\left(\frac{D}{\ell}\right)$$

Thin foil microscopy[19] and other experiments[10,20] suggest a reasonable value of $\left(\frac{D}{\ell}\right)$ to be of the order of 10.

4.3.4 Strain Due to the Operation of a Source

The strain associated with a source during its operation is given by

$$\epsilon = b.n.A/v \qquad (4.3)$$

where A = average area swept through by the dislocations, (cm^2); v = volume of specimen, (cm^3). Thus for unit volume $\epsilon = b.2\pi\left(\frac{D}{\ell}\right) \cdot \pi D^2$

$$= 2\pi^2\, b\left(\frac{D}{\ell}\right)^3 \cdot \ell^2$$

The minimum value of ℓ can be estimated by equating ϵ to the minimum detectable strain of 10^{-12}, calculated in Section 4.3.2.

or $$10^{-12} = 2\pi^2 \, b\left(\frac{D}{\ell}\right)^3 \ell^2$$

Substituting $\frac{D}{\ell} = 10$ and $b = 2.5 \times 10^{-8}$ we get $\ell \simeq 10^{-4}$ cm.

The above estimation shows that the minimum length of the Frank-Read source which is still able to produce a detectable burst is of the order of one micron for the detection sensitivity used in this investigation.

The model proposed above can be used to explain the observed acoustic emission behavior of various materials tested. The most significant observation is the emission from 2024 aluminum. In their as-received condition the bars were precipitation hardened; hence, in addition to the nodes of the Frank-network the dislocation segments are known to be further pinned by the hard precipitates which are distributed throughout the matrix at a spacing of about 150 to 400 A.(21) These precipitates effectively reduce the source length below the critical value of about one micron, hence during loading negligible emission is detected. When 2024 aluminum is heated to 975°F for four hours, water quenched and loaded immediately, large load emission is observed. The amount of this emission decreases progressively as the aging time at room temperature after water quenching is increased as shown in Figure (3.15). This can be explained as follows:

Heating at 975°F for four hours allows dislocations to form a stable network which has a length greater than 30 microns.(21) Alloying elements and impurity atoms go into solution and do not have time to precipitate out during water quenching. The impurities and alloying elements have only a weak pinning effect as explained in Section 4.3.1. The effective Frank-Read source length is therefore large enough to generate detectable emissions. Since 2024 aluminum alloy is precipitation hardenable at the room temperature, as the time after water quench-

ing increases the second phase precipitates out as small hard precipitates. These precipitates decrease the source length and thus decrease detectable emission. Overaging of this alloy causes the emission activity to return because the second phase particle agglomerate gives rise to a spacing of about 2.5 microns.[21] It is reasonable to believe that in the presence of such particles there may be a small number of dislocations which would have acquired the minimum critical length to produce the detectable emission. Because the particles are present in addition to the nodes in the Frank network, it is understandable that the emission count in Figure (3.16) is an order of magnitude smaller than for the solution heat treated condition. The observation that the air cooled and furnace cooled 2024 aluminum specimens do not produce any detectable emission can be rationalized because during these slow cooling processes there is plenty of time for precipitation of the particles to occur, thus reducing the source length to less than the critical value. The results of similar heat treatment processes on high purity aluminum (see Section 3.3.5) further support this argument. Because of the 99.99 percent purity there are not enough impurities to precipitate out during air cooling or furnace cooling, hence there is large emission from high purity aluminum regardless of the rate of cooling. The only treatment that eliminated the load emission for high purity aluminum was cold-working as reported in Section (3.3.5). It is reasonable to believe that the size of the Frank-network is reduced as a result of the cold-working so that the source length is less than the critical value required for detectable emission.

4.4 The Kaiser Effect

The phenomenon that the emission from a previously stressed material, does not begin until the previous stress is reached is known as the Kaiser effect.[4] In the light of the present investigation it is necessary to make the following qualification:

> If the material is in a favorable condition for giving out detectable load emission, and if it is not stressed beyond the point where the load emission ceases, such as point C in Figure 4.1, then the above mentioned Kaiser effect manifests itself (see Figure 3.12). However, once a material is stressed beyond the point where emission ceases there is no emission on subsequent stressing right up to the fracture point.

The model already presented can give an explanation for this behavior. When the material has sources longer than the critical length, the longest ones are activated first. As the applied stress increases, shorter ones start to become operative, and the emission activity continues to increase. During this process some of the sources are stopped due to the back stress of pileups, and some stop due to intersections caused by the generated dislocations from the neighboring sources. Some dislocations may still be capable of operating and generating detectable emissions, should the applied stress be increased. If, however, the material is unloaded at this point and is subsequently reloaded, then no source can operate until the previous stress level is reached. Further increase in stress causes some of the previously inoperative sources to become activated, thus giving out the detectable load emissions as evidenced by the Kaiser effect.

4.5 Shape of the Emission Amplitude Curve

The two opposing effects of increasing the applied stress as discussed in the last section are:

1. To cause progressively shorter sources to become operative.
2. To stop some of the previously operative sources with a resultant reduction of the number of sources capable of producing detectable emission. This number is likely to be further reduced due to the intersection of newly generated dislocation rings.

The first effect gives rise to an increased emission activity, and the second one tends to reduce it. At low stresses the first effect dominates and emission activity increases. However, as the applied stress increases, the second effect becomes more dominating, thus giving rise to a peaking emission amplitude curve (Figure 4.1). It can be argued that at the point C in the same figure all of the remaining dislocation sources have lengths smaller than the critical value, hence no emission activity can be detected.

4.6 Other Theories

It is significant to mention that Sedgwick[9] has proposed a similar model for the emission from LiF and KCl single crystals. He has suggested that the skewed parabolic emission curve is due to the symmetrical distribution of dislocation loop lengths. The emission activity decreases as a result of the exhaustion of sources at high stresses. The skew nature of the curve has been attributed to the greater number of smaller dislocations that become activated at higher stress. There seem to be three main objections to this belief:

1. It seems highly improbable that all of the sources cease to operate at the low values of the strain corresponding to the point where the emission stops (see Figure 4.6).
2. The absence of emission from a cold-worked material suggests that no dislocation multiplication should occur which once again does not seem to be acceptable in view of continued plastic deformation in this range.
3. When pileups overcome their barriers, the release of dislocations is likely to allow some of the sources to become operative again. If this is true, the emission activity should be revived. Observation of the Kaiser effect and the absence of emission from cold-worked materials do not agree with this deduction.

All of these questions may be resolved by the requirement of more than a minimum loop length to produce detectable emissions. Kerawalla[7] has suggested that the load emission in 1020 hot rolled steel, which coincides with the upper-lower yield point, is due to the unpinning of the dislocations from the carbon and nitrogen atoms. From the emission activity detected in the aluminum alloys and high purity aluminum, it can be concluded that unpinning from impurity atoms is not necessarily a requirement for the load emission. Further, strain aging of 1020 hot rolled steel after loading beyond the yield point brings back the yield drop, but not the load emission (see Figure 3.13). Hence, the model proposed by Fisher and Lally,[10] which suggests that emissions are due to the yield drop, seems doubtful.

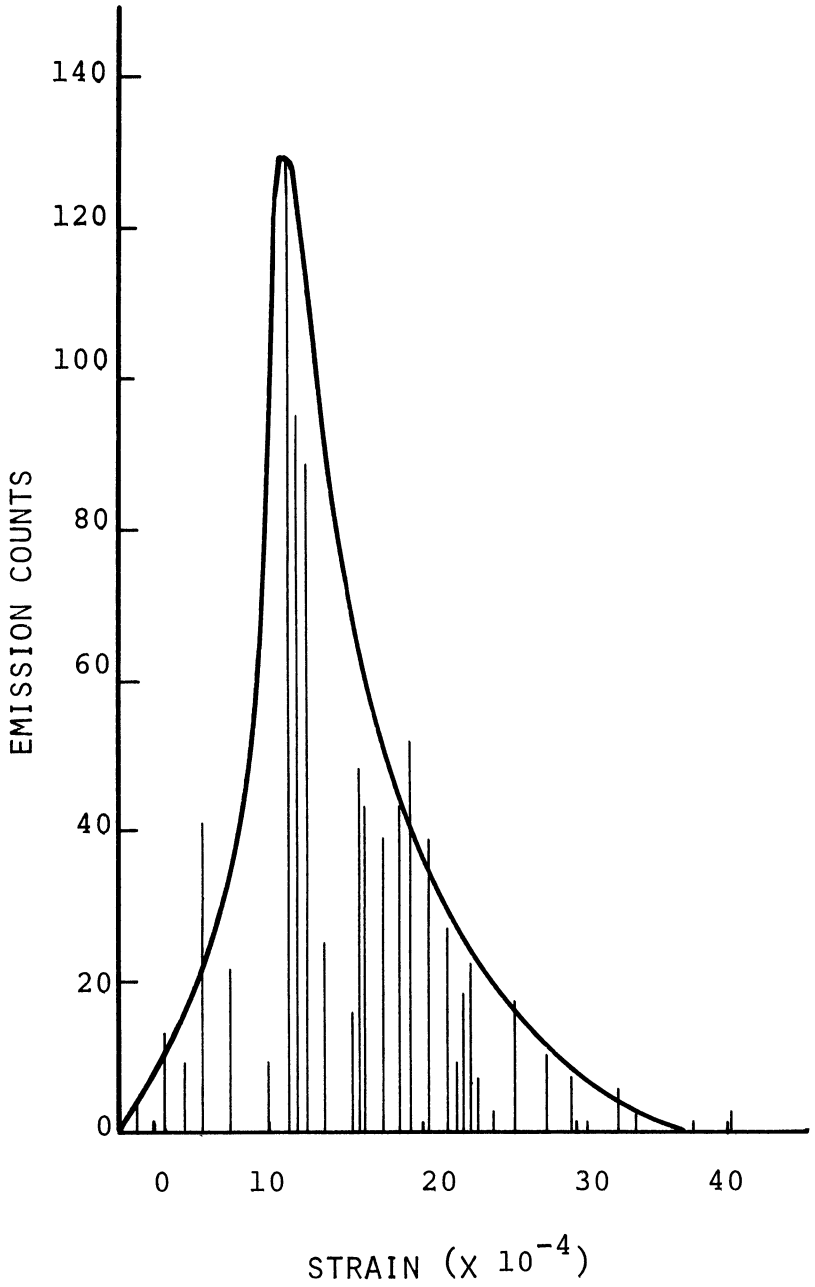

Figure 4.6 Acoustic Emission Histogram for LiF.[9]

The aging process can allow dislocations to get repinned due to the diffusion of carbon and nitrogen atoms. Hence, loading of strain-aged 1020 steel must cause dislocations to be unpinned in a manner similar to that in the hot rolled condition, as manifested by the revived sharp yield point. The absence of emission, therefore, would seem to indicate that in this case unpinning is not associated with the load emission.

Although 1020 steel has a relatively complicated structure, the model also seems to offer the plausible explanation that when the break-away stress is reached, dislocations start to tear away from the pinning points but are still held by the nodes of the Frank-network. Generation of dislocation loops can now begin producing detectable emission. After aging, emissions do not reappear because the size of the network becomes smaller due to the plastic deformation. The aging time (2 hours) and temperature (300°F) are not enough to allow dislocations to anneal out and rearrange themselves into a coarser network.

Schofield's[6] conclusion that acoustic bursts are due to the formation of stacking faults and mechanical twins seems questionable because 302 stainless steel, which has very low stacking fault energy and hence is more suited to the formation of stacking faults, shows very little burst activity compared with aluminum and 1020 steel which have much higher stacking fault energy.

4.7 Unload Emission

Although it is not possible to pinpoint exactly the source and the mechanism of the unload emission, the following discussion will help to highlight some of its salient features and characteristics.

Unlike the load emission, the unload emission is quite repeatable every time a specimen is unloaded after the same maximum stress has been induced. This suggests that the mechanism responsible for the unload emission should be reversible.

4.7.1 Size Effect

Figure 3.3(a) shows that the unload emission count increases almost linearly with the volume of the stressed section of the specimen. Surface finish and surface area of the specimens do not significantly alter the unload emission count as can be seen from Figures3.2 and 3.3(b). These observations suggest that the unload emission is due to an internal mechanism as opposed to being a surface related phenomenon.

4.7.2 Effect of Hardness

Tests on cold-worked and precipitation hardened aluminum alloys (see Figures 3.4 and 3.5) show that unload emission count increases as the hardness of the material increases. The almost total reversibility and increase in unload emission count with the increase in hardness seem to be quite contrary to what would be expected if one or more dislocation processes were to be responsible for the unload emission. It would seem, therefore, quite logical to consider a model based on the cleavage mechanism. Similarity of unload emission behavior in tensile and compressive loading modes (see Figure 3.9) suggests that the unload emission may not be due to the normal cohesive forces between the atoms. Hence, a shear type mechanism involving a reversible dislocation motion is more likely to explain the unload emission.

Figures 3.7 and 3.8 show that a large amount of unload emission is detected for a relatively small removal of load after specimens are

strain-aged within the grips under load. Emission activity becomes progressively lower for further reduction in applied loads.

When specimens strain-aged outside of the grips under identical conditions are stressed to the same extent and unloaded, the unload emission behavior is quite different. There is a period of no emission and further decrease in load causes increased emission activity as shown in Figure 3.8(b).

It seems reasonable to believe that strain-aging within the grips under load causes particles of the second phase and impurity atoms to diffuse to favorable sites in the vicinity of dislocations. Hence, during unloading, dislocations have to glide smaller distances before they meet obstacles.

In case of specimens which are already strain-aged loading causes dislocations to be torn away from the impurity atoms and second phase particles which are not able to diffuse to the vicinity of dislocations before unloading begins. These dislocations must, therefore, glide relatively longer distances before being obstructed.

This discussion suggests that the unload emission may be due to the impeding of the dislocation motion by obstacles when load is removed. Unload emission from the 99.99 percent purity aluminum, however, does not support this argument. Further, this model is not compatible with the model for the load emission.

From the foregoing discussion it is clear that the experimental observations of the unload emission behavior lead to conflicting inferences. Hence, it is felt that a reasonable speculation of a model to explain unload emissions must await further research.

CHAPTER V

CONCLUSIONS

On the basis of the experiments reported in this dissertation it appears possible to draw the following conclusions.

The principal cause of acoustic emissions detected during loading of materials appears to be due to the dislocation multiplication by the Frank-Read mechanism. Calculations show that only sources having lengths of the order of 10^{-4} cm. or greater are able to produce detectable emissions. This minimum detectable source length depends upon the sensitivity of the detection system used.

The model for the load emissions seems to be consistent with the existing work-hardening theories. It offers a plausible explanation for the phenomenon called "The Kaiser Effect" which has also been observed by numerous other workers. Absence of load emission from several materials with different processing history can be explained by this model.

It is not possible to propose a suitable model to explain the character of the unload emission. The following summary, however, seems to be appropriate:

1. The unload emission is highly repeatable in character for a given history of the material.
2. The unload emission count varies linearly with the volume of the stressed section of the specimen, and is almost unaffected by the surface area and surface finish of the specimen.

3. If the hardness of the material is increased, its emission activity on unloading is increased.
4. The cumulated unload emission count increases as the maximum stress reached is increased. In the elastic region the curve seems to be a straight line, but as the maximum stress reached increases beyond a certain value, the curve tends to level off as can be seen from Figure 3.6.
5. The unload emission behavior seems to be identical in tensile and compressive loading modes.
6. Aging within the grips under load causes an increased unload emission activity for a small removal of load.
7. Type 302 stainless steel gives off a much smaller amount of unload emission than the 1020 hot rolled steel and 2024-T6 aluminum.

The repeatable behavior and increase in unload emission counts with increased hardness appear to be incompatible with possible simple dislocation models. However, the similarity of unload emission behavior in tension and compression loading modes strongly favors a shear type mechanism involving dislocation motion. More research is needed to resolve this conflict.

The model for the load emission explains the behavior of the very particular materials tested and care should be taken not to draw conclusions that are too general. Nevertheless, since the testing covered a reasonable variety of materials and histories, it is felt that the model may be of help in understanding the material behavior in general.

CHAPTER VI

SUGGESTIONS FOR FUTURE RESEARCH

As a result of the experience gained during this investigation, it is felt that the acoustic emission phenomena seem to be worthy of further exploration as follows:

(1) Investigate means of obtaining a more direct correlation between the load emission and the critical size of the Frank-Read sources. It appears that thin film electron transmission microscopy may be able to provide worthwhile information.

(2) Increase the sensitivity of the detection system by an order magnitude or more. Based on the model proposed for the load emission, it should be possible to detect emission on loading from lightly cold worked materials. Likewise, it should be possible to detect load emission from precipitation hardened aluminum alloys.

(3) Study the load emission behavior by reducing the free length of dislocation sources by means other than cold-work, precipitation hardening or impurity atoms. One such method is the radiation hardening of high purity materials. The model proposed here predicts that the load emission should decrease substantially by such a treatment.

(4) Operation of dislocation sources gives rise to localized microstrain. Much can be learned by monitoring simultaneously the acoustic emissions and the microstrain.

(5) It appears that the upper-lower yield phenomenon in 1020 steel may be due to the larger stress required to break-away dislocations from the locking effects of C and N_2 solute atoms than the

stress required to operate the Frank-Read sources. This requires that dislocation line AB in Figure 6.1 should cross-slip to avoid repinning after a complete dislocation ring "0" has been generated so that the smaller stress is able to continue the operation of the sources, thus, accounting for the yield elongation. A microscopic investigation along these lines should be of immense value, in an attempt to explain the sharp yielding behavior of 1020 steel.

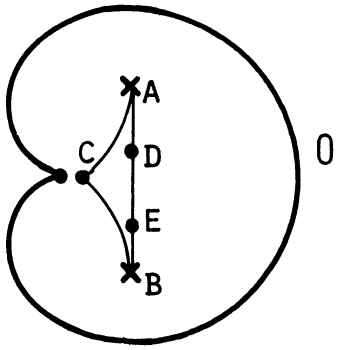

A AND B ARE NODES OF THE FRANK-NETWORK
D AND E ARE SOLUTE ATOMS OF CARBON AND NITROGEN
ACB DISLOCATION LINE AFTER RING 0 IS RELEASED

Figure 6.1 Operation of Frank-Read Source for a Possible Explanation of Yield Drop in 1020 Steel.

APPENDICES

APPENDIX I

INSTRUCTIONS FOR OPERATING ACOUSTIC EMISSION EQUIPMENT

1. Turn on the equipment by turning the main switch "on". Allow a few minutes for warm up.
2. Calibration of X-Y recorder:
   - 2.1 Calibration of X-axis.
     - a. Set the pen switch (standby reset switch) in reset position.
     - b. Keep the paper holder on.
     - c. Push galvanometer balance and adjust the zero knob of the X-axis for zero on the recorder.
     - d. Release the balance button and adjust the coarse and fine bridge balance to zero.
     - e. Push full scale calibration button and adjust X gain so that there is a deflection of 4.85 in on the recorder. This completes the X-axis calibration.
   - 2.2 Calibration of Y_1-axis:
     - a. Set the switch on the vacuum tube voltmeter to "VTVM" position and the toggle switch of position deflection box to "off".
     - b. Adjust zero knob for Y_1 so the pen is set at zero deflection (top line on the graph sheet placed on the recorder).
     - c. Set the range knob on the voltmeter for 0.03V and switch the knob on the calibration box to "Calibrate" position.
     - d. Turn the switch on the vacuum tube voltmeter to "AMP" position.
     - e. Adjust the gain of Y_1 until a 5" deflection is obtained.

f. Turn the position deflection toggle switch to "on" and adjust so that the deflection is 1".

2.3 Calibration of Y_2-axis

a. Set the Digital-to-Analog converter to "galvonometer zero" position.

b. Adjust the Y_2 zero knob for zero deflection on recorder.

c. Set the Digital-to-Analog converter to "calibrate" and adjust the gain on Y_2 for 5" deflection on recorder.

d. Turn the Digital-to-Analog converter to "operate".

3. Calibration of Digital Counter:

a. Turn the Voltmeter knob to 0.1 volt and the switch to VTVM position.

b. Turn the switch on the calibration box to "trigger set". The voltmeter now reads RMS trigger voltage.

c. Set the "level A" knob on the counter so that the counter just triggers. This completes the calibration of the digital counter. Turn the voltmeter switch to "AMP" position and the range switch to 0.03 V position. Turn the calibration box switch to "RUN" position. When calibrated properly the scales for the axes are as follows:

X-axis	500 pounds/inch
Y_1-axis	5mV/inch
Y_2-axis	2000 counts/inch

APPENDIX II

PROCEDURE FOR CHECKING THE ACOUSTIC LOADING MACHINE FOR EXTRANEOUS NOISE

In order to ensure that the acoustic emission data are valid and reasonably uninfluenced by extraneous noise, following components of the loading machine were checked for noise.

(1) Tanks No. 2 and No. 3 were checked for rubbing by putting the crystal transducer on it and then lowering and raising tank No. 1 so as to move tank No. 3 up and down. The output of the transducer revealed that there is no rubbing between tanks No. 2 and No. 3. No specimen was placed in the grips during this test. Similar tests were conducted by putting the detector on the grips to ensure quiet operation of the loading mechanism.

(2) In order to ensure that the emission was not due to the rotation of the specimen in the grips, experiments were performed on the same setup by Tom Radkevich (unpublished) by gluing the specimen in the grips by epoxy cement. It was found that the gluing does not alter the emission behavior significantly. Complete absence of load emission from an already stressed material further shows that there was no significant extraneous noise.

APPENDIX III

MISCELLANEOUS EXPLORATORY EXPERIMENTS

The following paragraphs describe some experiments that were performed during the investigation which are not directly related to the main objectives of the work. They are being reported because of their general interest. No conclusions have been drawn from these.

A-3.1 Effect of Lowering the Temperature of the Specimen on the Unload Emission

6061 aluminum and 1020 steel specimens were used for this test. The pick-up head was mounted on the specimen and the assembly was then soaked in a flask containing liquid nitrogen for several minutes until the liquid nitrogen stopped boiling. The specimen was then quickly placed in the grips and loaded and unloaded. A number of loading and unloading tests were performed until the specimen reached the room temperature. Results indicate that the unload emission count decreases as the temperature of the specimen is lowered. No attempt was made to measure the specimen temperature as it was changing continously during this experiment. At a temperature close to that of the liquid N_2 (-196°C) the emission on unload was about one half of that of the unload emission at room temperature.

A-3.2 Effect of the Strain Rate on Unload Emission

The rate of loading was varied by partly closing valve No. 1 (Figure 2.1) thus controlling the rate of flow of water in and out of the Tank No. 3. Tests on 6061 aluminum specimens show thatthe decrease in the unloading rate from 100 pounds per second to about 1.5 pounds per second reduces the unload emission from 4,000 to 2,500 counts.

LIST OF REFERENCES

1. Orowan, E., Z. Physik, 89, p. 605, 1934.

2. Taylor, G. I., "Mechanism of Plastic Deformation of Crystals," Proc. Roy. Soc. (London), A, 145, p. 362, 1934.

3. Polanyi, M., Zeit fuer Physik, 89, p. 660, 1934.

4. Kaiser, J., "Untersuchungen Uber das Auftreten von Gerauschen biem Zugversuch," A doctoral dissertation presented to Fahultet fur Waschinenwesen und Elekrotechnik Der Technischen Hochschule Munchen, Munchen, Germany, 1950.

5. Liptai, R. G., and Tatro, C. A., "Acoustic Emission-A Surface Phenomenon," Symposium on Nondestructive Testing of Aircraft and Missle Components, 1962.

6. Schofield, B. H., Acoustic Emission Under Applied Stress, Report No. ASD-TDR-63-509, Part II, Wright Patterson Air Force Base, May 1964.

7. Kerawalla, J. N., "An Investigation of the Acoustic Emission From Commercial Ferrous Materials Subjected to Cyclic Tensile Loading," Doctoral Thesis, The University of Michigan, October 1, 1965.

8. Mitchell, L. D., "An Investigation of the Correlation of the Acoustic Emission Phenomena and the Scatter in the Fatigue Data," Doctoral Thesis, The University of Michigan, October 1, 1965.

9. Sedgwick, R. T., "An Investigation of Acoustic Emission From Coated and Uncoated Ionic Crystals," Doctoral Thesis, Michigan State University, 1965.

10. Fisher, R. M., and Lally, J. S., "Microplasticity Detected by an Acoustic Technique," Canadian Journal of Physics, Vol 45, 1967.

11. Frank, F. C., "The Origin of Dislocations," Pittsburgh Conference, O.N.R., p. 89, 1950.

12. Mott, N. F., "A Theory of Work Hardening of Metal Crystals," The Philosophical Magazine, Vol. 43, October 1952.

13. Cottrell, A. H., and Bilby, B. A., Proc. Phys. Soc. (London), Vol. 62A, pp. 49-62, 1949.

14. Suzaki, T., and Imura, T., Phys. Soc. (London), 1954.

15. Cottrell, A. H., "The Yield Point in Sincle Crystals and Polycrystalline Metals," Pittsburgh Conference, O.N.R., p. 60, 1950.

16. Friedel, J., Dislocations, Addison-Wesley, p. 239, 1967.

17. Frank, F. C., and Read, W. T., "Multiplication Processes for Slow Moving Dislocations," Symposium on The Plastic Deformation of Crystalline Solids, Pittsburgh, 1950.

18. Granato, A., and Lucke, K., "Application of Dislocation Theory to Internal Friction Phenomena at High Frequencies," Journal of Appl. Phys., Vol. 27, No. 7, p. 583 and 789, 1956.

19. Hirsh, P. B., and Lally, J. S., "The Deformation of Magnesium Single Crystals," Phil. Mag., Vol. 12, p. 595, September 1965.

20. Hazzledine, P. M., "Work Hardening in Easy Glide," Canadian Journal of Physics, Vol. 45, p. 765, February 1967.

21. Greetham, G. and Honeycombe, R.W.K., "The Deformation of Single Crystals of Aluminum - 4.5 Percent Copper Alloy", J. Inst. Metals, 89, (1960-61), 13.

22. Hull, D., "Introduction to Dislocations," Pergamon Press, p. 248, 1965.

23. Kaiser, J., Archive fuer das Eisenhuttenivesen, 1, (also Doctoral Thesis), 1953.

24. Schofield, B. H., Acoustic Emission Under Applied Stress, Report No. ASD-TDR-63-509, Part I, Wright Patterson Air Force Base, April 1963.

25. Schofield, B. H., Proceedings of the Symposium on Physics and Nondestructive Testing, San Antonio, Texas, Sponsored by Southwest Research Institute, October 1963.

26. Koehler, J. S., Imperfections in Nearly Perfect Crystals, John Wiley and Sons, Inc., New York, p. 197, 1952.

27. Borchers, H., and Tensi, H., Zeit fur Metallkunde, 53, No. 10, pp. 692-695, 1962.

28. Borchers, H., and Tensi, M., Zeit fur Metallkunde, 51, No. 4, pp. 212-218, 1960.

29. Schofield, B. H., Bareiss, R. A., Kyrala, A. A., Acoustic Emission Under Applied Stress, Lessells and Associates, Inc. WADC Technical Report 53-194, 1953.

30. Schofield, B. H., and Bareiss, R. A., Acoustic Emission Under Applied Stress, Progress Report No. 1, Contract No. AF 33(616)-5640, WADC, Ohio.

31. Schofield, B. H., Acoustic Emission Under Applied Stress, Progress Report No. 2 through 11, Contract No. AF 33(616)-56 0, WADC, Ohio.

32. Tatro, C. A., Sonic Techniques in Detection of Crystal Slip in Metals, Division of Engineering Research, Michigan State University, January 1959.

33. Tatro, C. A., and Liptai, R. G., Acoustic Emission from Crystalline Substances, Symposium on Physics and Nondestructive Testing, October 1962.

34. Dunegan, H., Tatro, C., and Harris, D., Technical Paper, University of California, Lawrence Radiation Laboratory, November 1964.

35. Kroll, R. J., "Stress Waves in Test Specimen Due to Simulated Acoustic Emissions," Doctoral Thesis, Department of Applied Mechanics, Michigan State University, 1962

36. Czochralski, J., Steel and Iron, (1917), p. 502.